Developing a 3D Model Geometry of the Hikurangi Subduction Zone

Eva Bijlsma

February 2024

Abstract

The Hikurangi subduction zone, located off the east coast of the North Island of New Zealand, has not seen a large ($M_W \geq 8.0$) megathrust earthquake in recent history. This does not mean that great earthquakes are not possible on the subduction thrust. The seismic hazard of the Hikurangi margin can be assessed by determining where on the plate contact slip deficit is accumulating during the interseismic period. This can be done by comparing surface velocities produced by a 3D mechanical model to actual GPS data, changing locking configurations to determine the best fit. This study is the first part of a multi-step project on interseismic coupling at the Hikurangi Subduction Zone. This first part focuses on building a 3D model geometry that represents the Hikurangi margin. This geometry was constructed using Gmsh (Geuzaine and Remacle, 2009). The subducting slab is based on Slab2 (Hayes et al., 2018) and varies along both strike and dip. The overriding plate is simplified, with constant thickness and no topography. The geometry also includes a cold nose, mantle wedge and sub slab mantle. To test the geometry, two models are compared to each other, one where the subducting slab is stably sliding without resistance and another where a circular feature on the megathrust with a diameter of 50 km is coupled to the overriding plate or 'locked'. Displacement and slip on the megathrust are considered as well as the accumulation of shear traction on the slab's surface. Finally horizontal surface velocities produced by locking are compared to GPS velocities. The results show that the locking is functional and that locking has a far-reaching, mechanically continuous influence on displacement in the model. Overall it can be said that the model geometry is ready for the next step of this project.

1 Introduction

Subduction zones are capable of producing great earthquakes that cause significant damage. These earthquakes originate due to stick-slip behaviour on the plate contact between the downgoing and overriding plates, also called the megathrust. During the period between two earthquakes, the interseismic period, stress builds up on the megathrust, to be released during the next earthquake. The interseismic period can have a duration of anywhere between several days to several hundreds of years. Megathrust earthquakes can have very large magnitudes, like the 2011 M_W 9.0 Japan earthquake (Wallace et al., 2014). Along the Hikurangi margin, located off the east coast of the North Island of New Zealand, there is no historical record of large ($M_W \geq 8.0$) megathrust earthquakes. The length of the interseismic period (the recurrence interval) of such megathrust earthquakes is estimated to be between 300 (Wallace et al., 2009) and 875 years (Reyners, 1998). The historical record goes back only 180 years (Wallace et al., 2014). Because of this relatively short historical record, the lack of records on large megathrust earthquakes does not necessarily mean that there will not be any in the future. The seismic hazard of the Hikurangi margin therefore needs to be estimated with different methods, such as determining slip deficit accumulation. This is calculated by subtracting the slip on the plate interface from the relative motion of the plate (Herman et al., 2018). To determine where the potential for hazardous earthquakes is the largest, it is important to know where on the subduction thrust a slip deficit is accumulated.

1.1 Tectonic Setting

New Zealand is located in the plate boundary zone of the Pacific and Australian plates (figure 1). Processes related to this zone dominate its active tectonics. Below the North Island of New Zealand, the oceanic Pacific Plate is subducting westward beneath the continental Australian Plate at the Hikurangi margin (Wallace et al., 2009). At the trough, off the east coast of the North Island, the subducting lithosphere has an age of 120 Myr and a thickness of 118-132 km (Hayes et al., 2018). Its crustal component is an oceanic plateau, the Hikurangi Plateau, which has a thickness of 10-15 km (Davy and Wood, 1994). The velocity of the Pacific plate relative to the Australian plate ranges from 47 mm/y in the north, at an angle of $\sim 70^\circ$ to the trough (DeMets et al., 2010; Reyners et al., 2011), to 37 mm/y nearly trench parallel around 42°S (DeMets et al., 1994; Reyners, 1998).

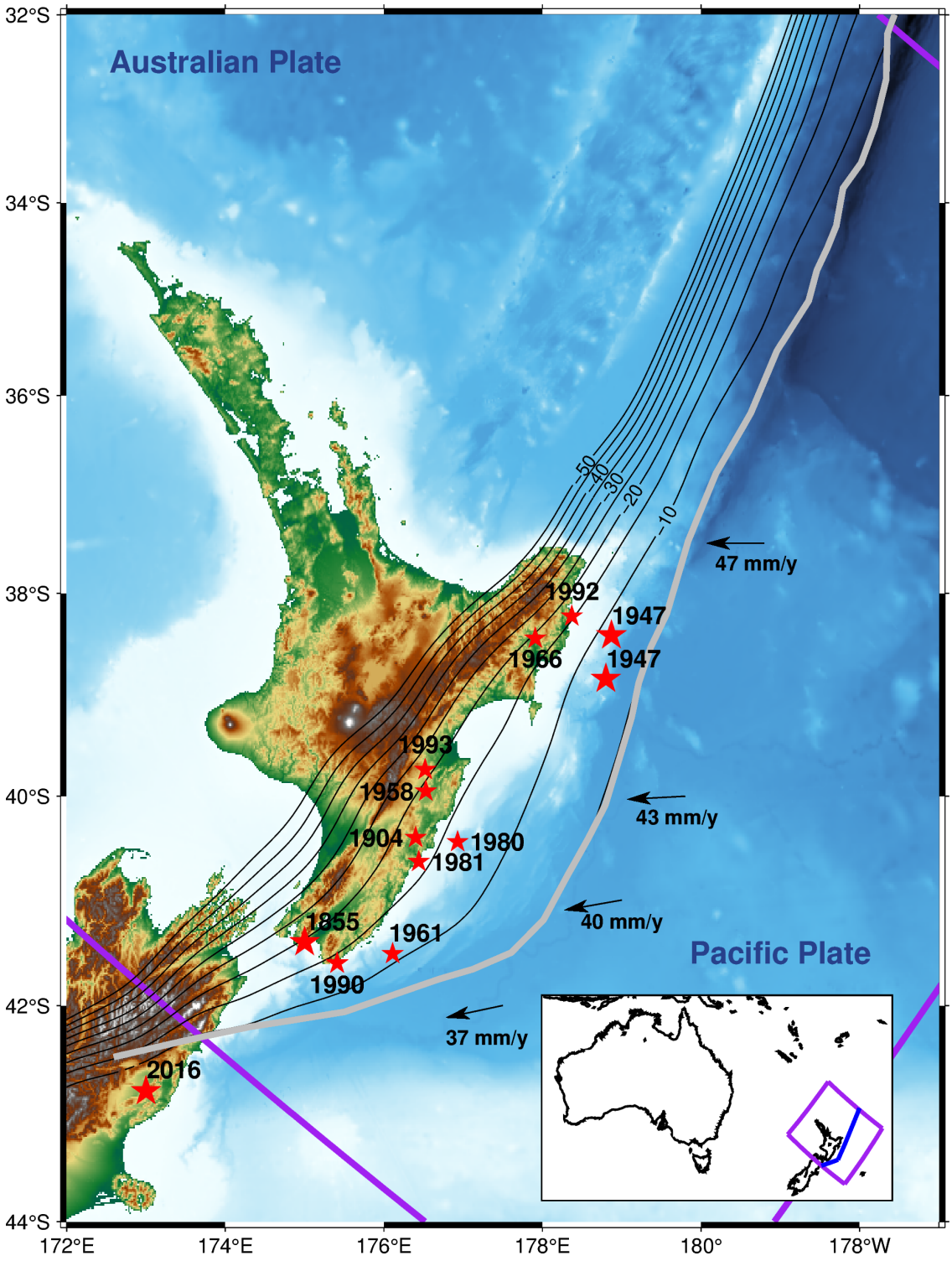

Figure 1: Topographic map of the North Island of New Zealand and part of the South Island with contours of the top of the subducting plate in black. The grey line marks the trench (Bird, 2003) on the main map, the blue line in the inset is a simplified version that is used in the model geometry. The boundaries of the model are in purple both on the main map and the inset. The direction of Pacific Plate motion is shown by the arrows. Red stars mark epicenters of significant earthquakes. Their size indicates their relevance: earthquakes that are directly mentioned in the text have larger stars than those mentioned only indirectly. Earthquake epicenters are from Doser and Webb (2003), Furlong and Herman (2017), Wallace et al. (2014), and Webb and Anderson (1998).

Subduction ceases around 42.5°S where there is continental crust on both sides of the margin: the Chatham Rise and the Challenger Plateau (Beavan et al., 2002; Wallace et al., 2009). There, the Marlborough Fault Zone connects the Hikurangi margin to the Alpine fault, an oblique transform plate boundary running through the South Island (Zachariasen et al., 2006). Northwards, the Hikurangi trough connects to the Kermadec and Tonga trenches. Together, they form a subduction system that is 3000 km long (Wallace et al., 2009). Volcanism related to back-arc spreading is concentrated in the Taupo Volcanic Zone (TVZ), located north of 39°S on the central North Island (Wallace et al., 2009). The extension rates of the TVZ increase northward from <5 mm/y around 39°S to 15.6 mm/y around 38°S (Wallace et al., 2004). Evidence of compressive tectonics has been found south of 39°S (Stern et al., 2006). Shortening has been estimated at ∼4 mm/y (Wallace et al., 2004). According to Wallace et al. (2004) the contrast between back-arc extension and compression is caused by variations in thickness of the Hikurangi Plateau. The thicker (15 km thick) crust in the south leads to collision, while thinner (10 km thick) crust allows for slab rollback to happen, which can cause extension. The geodetic signature of the subducting slab in combination with extension in the north and compression in the south leads to a GPS velocity field that resembles a clockwise rotation relative to the Australian plate (figure 2). Clockwise rotation of the North Island has been studied with geodetic (Wallace et al., 2004) and paleomagnetic (Mumme et al., 1989) data as well as by tracking volcanic arc migration (Calhaem, 1973). Rotation rates between 0.44°/Myr and 7°/Myr relative to the Australian plate, depending on the used method, have been reported, with rotation poles clustering around 173°E, 39.5°S. The rotation is believed to accommodate part of the margin-parallel component of the oblique subduction at the Hikurangi margin. The remaining motion is accommodated on strike-slip faults on the overriding plate (Wallace et al., 2004). A combination of slip on the plate interface and upper plate shortening accommodates the margin-normal component of the oblique subduction. On geologic timescales, the margin-normal component of subduction is mostly accommodated by slip on the subduction thrust ($\geq$80%), with a small part being partitioned into shortening of the overriding plate. On shorter timescales, however, GPS data show that there is less slip on the subduction thrust (20%) and more shortening. This difference suggests that motion on the plate contact between the Pacific and Australian plates is characterized by stick-slip behaviour (Nicol and Beavan, 2003).

1.2 Seismicity

New Zealand's earthquake history goes back approximately 180 years. Since then, most earthquakes around the Hikurangi margin have been on upper plate faults (Clark et al., 2015). Earthquakes from before the 1840s are only documented in Māori oral history, which makes it difficult to associate these earthquakes with a precise source (Wallace et al., 2014). Because of the large number of upper plate faults near the Hikurangi Margin, it is still complicated to determine the source fault of each earthquake, even with modern seismic networks. The effects of earthquakes on the nearby faults being similar to those of an interface rupture, like coastal deformation or tsunamis, adds complexity as well (Clark et al., 2019). Earthquakes can also involve rupture on both the subduction interface and upper plate faults. An example of this is the 2016 M_W 7.8 Kaikōura earthquake (Furlong and Herman, 2017), which generated a tsunami with waves up to 4 meters high (Clark et al., 2019). The earthquake originated on an upper plate fault but the tsunami was caused by oblique low-angle thrusting, which is associated with the megathrust. The event triggered afterslip and slow slip events on the interface as well (Wallace et al., 2018). Since the installation of the seismic network in 1917, there have been several earthquakes (partly) caused by rupture on the subduction interface (figure 1). Two significant earthquakes during this period are the March 1947 Poverty Bay earthquake, measuring M_W 7.0-7.1, and the May 1947 Tolaga Bay earthquake, measuring M_W 6.9-7.1. The March and May 1947 earthquakes both caused tsunamis that were large relative to the magnitude of the earthquakes and are associated with the locations of subducting seamounts. Other significant earthquakes that are with certainty attributed to the interface have magnitudes 5.5-6.5 (Wallace et al., 2014). The 1855 Wairarapa earthquake, which happened before the possibility of instrumental measurements but has estimated M_W 8.1-8.4, could have involved slip on the subduction interface as well as on the Wairarapa fault. This is based on evidence of vertical motion near Wellington related to the earthquake. However, this vertical motion was not extensive enough to confirm the involvement of the subduction thrust in this earthquake (Beavan and Darby, 2005). For earthquakes that happened before historic records were established, geological data can be used to determine involvement of the subduction thrust. Evidence of uplift, subsidence and tsunamis shows 10 possible subduction earthquakes in the last 7000 years. The most recent rupture is estimated to have been 470-520 years ago on the southern part of the margin (Clark et al., 2019).

1.3 Previous work

Several methods have been used to estimate the slip deficit/ degree of interseismic coupling of the Hikurangi subduction zone. The first method compares GPS surface velocities with the plate velocities of the Australian or Pacific plates, assuming that this is a measure of the build-up of elastic strain on the plate interface (Wallace et al., 2009). When the subducting plate slides stably without resisting forces, the GPS velocities on the overriding plate are not impacted by the subduction. When part of the interface is locked, however, the overriding plate will be dragged along with the subducting slab until the interface ruptures and an earthquake occurs.

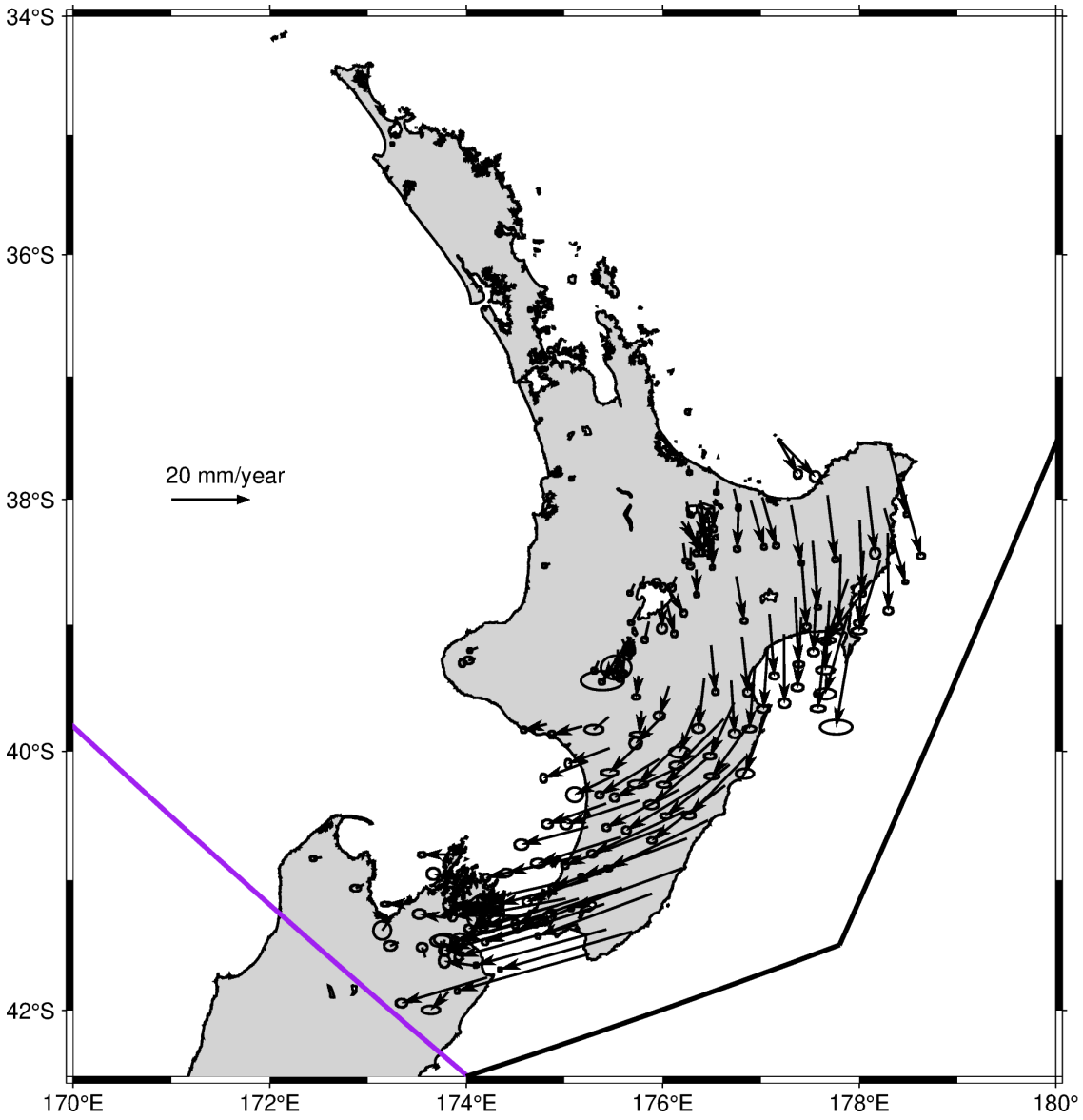

Figure 2: Map of the North Island of New Zealand with horizontal GPS velocities (Blewitt et al., 2016, 2018). The purple line shows the southernmost model edge and the black line the model trench (based on Bird, 2003).

This dragging of the overriding plate affects surface velocities on the overriding plate, directing them landward, which is why GPS can be used to estimate the degree of interseismic coupling. Another method uses the hypocenters and arrival times of past earthquakes (Reyners, 1998) to approximate the slip deficit. A record of large earthquakes implies that there will be more. This approach is based on the assumption that larger earthquakes equal more coupling (Ruff and Kanamori, 1980). In the case of the Hikurangi margin this method is not very reliable as the historical record of earthquakes is relatively short (∼180 years) while the return period of great megathrust earthquakes in the region is estimated to be at least 300 years (Reyners, 1998; Wallace et al., 2009), but could be up to 625 (Wallace et al., 2009) or even 875 years (Reyners, 1998) for a M_W 8.0 earthquake on the southern North Island. In other words, that there is no record of an interface rupture with $M_W \geq 8.0$ does not mean that these great ruptures are not possible along the Hikurangi margin. Smaller earthquakes and microseismicity may indicate regions with lower coupling, as the buildup of energy is released more often or even continuously (Wallace et al., 2009). Using slow slip events (SSEs) is another way to further constrain the edges of the regions with strong interseismic coupling. Slow slip events are a type of plate movement somewhere between an earthquake and a stably sliding fault: episodic like an earthquake but not fast enough to produce seismic waves (Dragert et al., 2001; Wallace, 2020). SSEs have been observed at several subduction zones around the Pacific Plate where other methods (geodetic and seismological) have determined to be the transition zone between strongly coupled and weakly coupled regions (Dragert et al., 2001; Hirose et al., 1999; Schwartz and Rokosky, 2007). Therefore, they are believed to be able to help constrain the location, geometry and extent of the locked regions on the Hikurangi subduction interface (Wallace et al., 2009). Along the Hikurangi margin specifically, the nature of SSEs varies with location. The locations of SSEs compared to the pattern of interseismic locking based on GPS velocities, are used as confirmation of the validity of this pattern. Slow slip events in New Zealand generally occur on what are believed to be the edges of strongly coupled regions.

Reyners (1998) proposed a crude locking pattern based on arrival time inversions of (micro)earthquakes and focal mechanisms together with geologic and geodetic data. The northern South Island was suggested to be permanently locked, which means that the Pacific plate would not be actively subducting there. Towards the north, the pattern shows a transition from strong locking on the southern North Island, via moderate/ weak coupling around Hawke's Bay (central North Island), to weak coupling beneath the northern North Island. According to Reyners (1998) this transition is caused by thickness variation in both the downgoing (thick in the south, thin in the central and northern regions) and overriding (thick in the south and central regions, thin in the north) plates. Darby and Beavan (2001) proposed that the southern North Island is almost fully locked (coupling coefficient close to 1.0). In Wallace et al. (2004) a more detailed locking pattern was suggested based on geodesy and tectonic block rotations. In this model, the transition from a coupling coefficient close to 1 (stronger locking, in the south and of the east coast of New Zealand in the north) to a coupling coefficient close to 0 (weaker locking, in the north) is very sharp. Contrary to Reyners (1998), the interface beneath northern South Island has a low coupling coefficient and thus is not locked. Wallace et al. (2012) refined the locking pattern from 2004, resulting in a similar pattern but with a more continuous strip of strong locking off the east coast of the North Island and a slightly lower slip deficit beneath the southern North Island. The transition from high to low coupling is still abrupt though. This locking pattern suggests that the southern North Island of New Zealand is at risk for large megathrust earthquakes and tsunamis, perhaps even similar to the 2011 M_W 9.0 Japan earthquake, while the risk is lower on the northern North Island (Wallace et al., 2014).

1.4 Aim

According to previous workers (Wallace et al., 2004, 2012) only the southern portion of the Hikurangi subduction interface is fully coupled to the overriding plate (and thus accumulates slip deficit), posing significant earthquake risks. The northern portion of the interface is believed to be almost fully uncoupled, with a sharp transition between the coupled and the uncoupled zones. A sharp transition between areas with contrasting slip rate deficits is not in agreement with continuum mechanics, as a patch that is locked will slow down its surroundings (Herman et al., 2018). As a result, earthquake potential may be underestimated for the northern North Island. Past research on the Hikurangi margin has not yet included a 3D mechanical model that focuses on interface locking. Considering that GPS velocities are 3D it is most accurately compared with a model that produces 3D velocities as well. Therefore, a 3D model with a detailed and accurate model geometry, especially regarding the subducting slab, is best suited to determine whether the conclusion that the interface beneath the northern North Island is not (fully) coupled is correct, and if not, if this locking poses earthquake risks. A comparison between surface velocities resulting from locking part of the interface and GPS data from New Zealand's continuously operating GPS network (Beavan et al., 2016, see figure 2) can aid in determining which locking configurations are likely in light of existing observations. GPS data are obtained from Blewitt et al. (2018) and Blewitt et al. (2016). Creating this model is a multi-step project, and the aim of this first sub-project is to construct a 3D model geometry based on the Hikurangi subduction zone with the option to lock part of the megathrust. The model with locking will have to show significant surface velocities on the overriding plate, as interface locking is believed to (at least partly) be the cause of the GPS velocity field (Wallace et al., 2012).

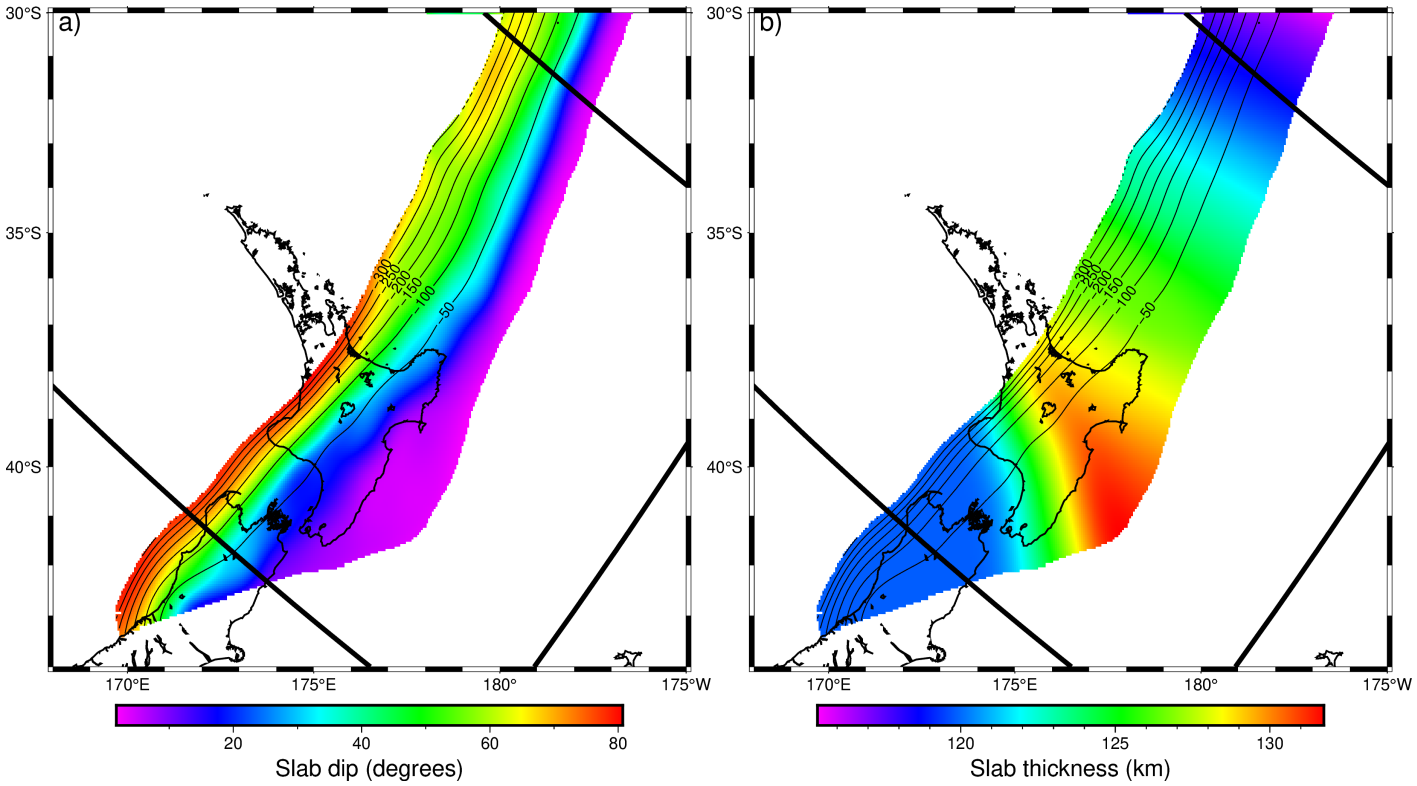

Figure 3: Two maps of New Zealand with Slab2 data (Hayes et al., 2018) imposed on top, a) shows the slab depth (contour lines) and dip (colors) and b) slab depth (contour lines) and thickness (colors). The thick black lines in a) and b) show the model's edges.

2 Model set-up

The process involves the construction of a 3D geometry based on the Hikurangi margin, which is used in a finite element model. The subducting slab in this geometry is based on actual data (Slab2, Hayes et al., 2018), making it variable both along dip and along strike (figure 3). Slab2 is a model of the geometry of all seismically active subduction zones, including the Hikurangi subduction zone. It uses active source seismic data, receiver functions, seismic tomography and both local and regional seismicity (Hayes et al., 2018). It specifically includes studies that were executed along the Hikurangi margin (Barker et al., 2009; Sutherland et al., 2009; Williams et al., 2013). Other model parameters are based on previous mechanical subduction zone models (Govers et al., 2018; Herman and Govers, 2020b; Herman et al., 2018) and studies on the Hikurangi subduction zone (Beavan et al., 2016; Bird, 2003; Tesauro et al., 2012) and subduction zones in general (Abers et al., 2020; Luo and Wang, 2021). The model geometry is constructed using Gmsh (version 4.10.5 (Geuzaine and Remacle, 2009)), making use of the OpenCASCADE kernel. Gmsh is chosen because of its ability to generate detailed 3D finite element meshes. The finite element code used is GTECTON (version 2023.dev, Govers and Wortel, 2005). The resulting model has an option to lock part of the slab to simulate the accumulation of slip deficit which could potentially result in a megathrust earthquake. The results of this work will show a comparison between two models, a reference model which is fully unlocked (i.e. stably sliding) and a model where a circle-shaped part with a diameter of 50 km (called an asperity) is coupled to the overriding plate, with its surroundings still stably sliding.

2.1 Domain boundaries

The area of interest, the North Island of New Zealand and the Hikurangi margin, is located between 34.5 and 42° S and 170 and 180° E. Within this area, all GPS stations on the North Island are included (figure 2). Where possible, the domain boundaries are chosen widely around this area of interest to avoid domain boundary artefacts. The easternmost boundary of the model geometry is at least 300 km from the trench, which is far enough based on studies with similar purposes (Herman and Govers, 2020b; Herman et al., 2018), where distances of at least 100 km between the trench and the edge of the model are used. To the west, the model domain extends 300 km from the westernmost point of New Zealand's coastline, and around 750 km from the TVZ, from where GPS velocities approximate zero westward (figure 2).

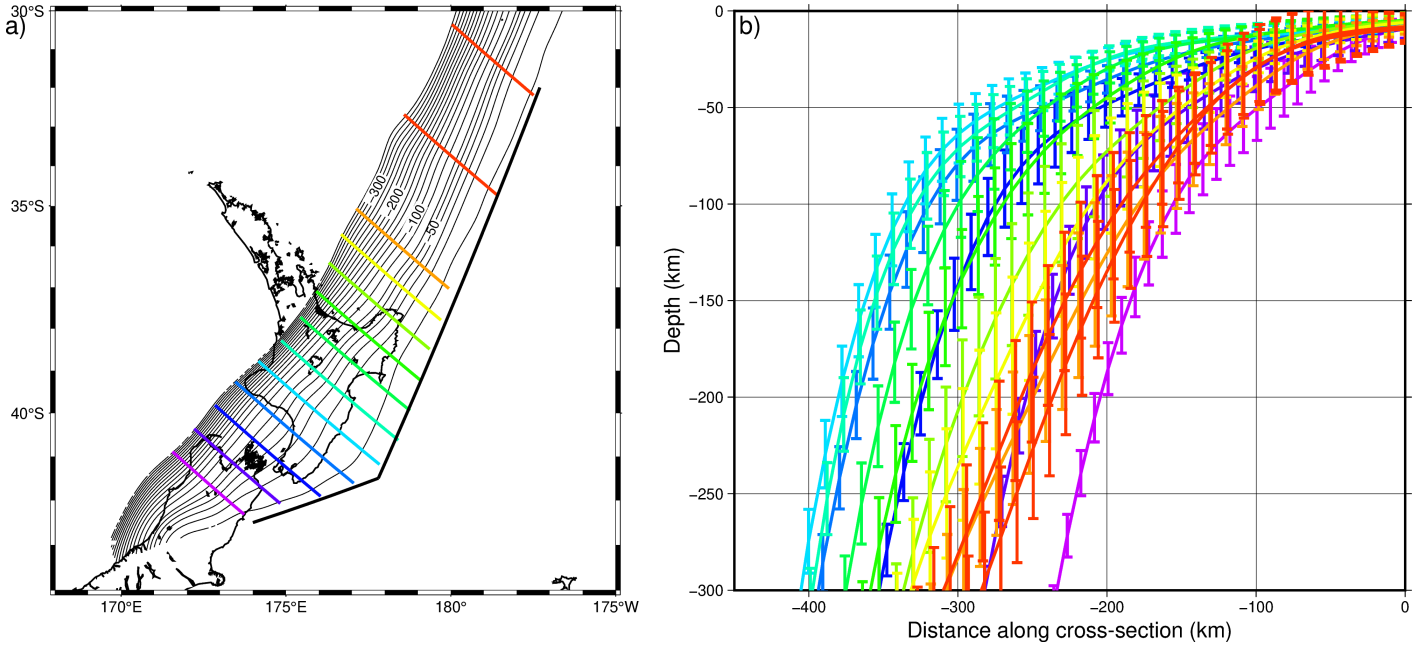

Figure 4: a) Map view of the locations of the cross-sections through the Slab2 data (Hayes et al., 2018) used to approximate the slab geometry. The contour lines show the depth of the slab and the thick black line is the model trench (based on Bird, 2003). The colors of the cross-sections correspond to b), where their shape is shown including error bars. The purple line is the southernmost edge of the model and the red line the northernmost edge.

Northwards, the model extends 700 km beyond the edge of the research area. The Hikurangi margin terminates at 42.5°S and transitions into the Alpine Fault (Beavan et al., 2002; Wallace et al., 2009). Extending the subduction zone further southwards than 42.5°S would not be accurate and including the South Island in a realistic manner would complicate the model, which was not preferred. Figure 3a shows that the shape of the slab changes significantly south of 42°S. The slab dip increases rapidly and the slab seems to be pinched off. To avoid warping the slab geometry unnecessarily the southern boundary of the domain was chosen to be adjacent to the area of interest. As a consequence domain boundary artefacts may not be prevented. The northern and southern model boundaries are parallel to cross-sections which were chosen to be approximately perpendicular to the overall strike of the slab at depths greater than 100 km. Close to the surface the strike varies, as does the shape of the trench, but at greater depths the strike is fairly uniform (contour lines in figure 4a, Hayes et al., 2018). The overall model is 1350 by 1400 by 298 km. The model origin (x,y,z) = (0,0,0) is located at 39° S, 176° E and the free surface. The positive x-axis points to the southeast, the positive y-axis points northeast and the positive z-axis points upwards.

2.2 Geometry

2.2.1 Pacific plate

To approximate the shape of the downgoing slab at the Hikurangi margin, thirteen cross-sections were made through the Slab2 data (Hayes et al., 2018), which are shown in figure 4a. Eleven of these cross-sections are equally spaced within the model domain. Of the remaining two, one defines the slab along the northernmost edge of the model, the other controls the shape of the slab between its adjacent cross-sections (the two red lines in figure 4a). The data points of these cross-sections are used to construct the slab's top surface. The shapes of the cross-sections are plotted in figure 4b, together with their vertical uncertainties. Horizontal uncertainties are not included in Slab2 (Hayes et al., 2018). The figure shows that the slab is curved. Its northern and southern ends are the steepest. Using only the two cross-sections at the edges therefore does not approximate the shape of the slab well enough, as the center cross-sections have gentler slopes. Figure 4b shows that most neighbouring cross-sections are similar enough that they fall within each other's vertical uncertainties. In the south where the trench curves and approaches the transition into the Alpine Fault, the error bars overlap less. Since the shape becomes gradually steeper in the south (i.e. apart from this steepening the actual shape of the slab does not change significantly), interpolation between the cross-sections approximates the slab surface. For most of the cross-sections, the Slab2 (Hayes et al., 2018) depth data start at 5-8 km depth and do not intersect with the trench (figure 4b). The slab's surface east of the trench was chosen to be constant at 3.2 km depth, based on the ocean depth of the coast of Hawke's Bay (Google Earth).

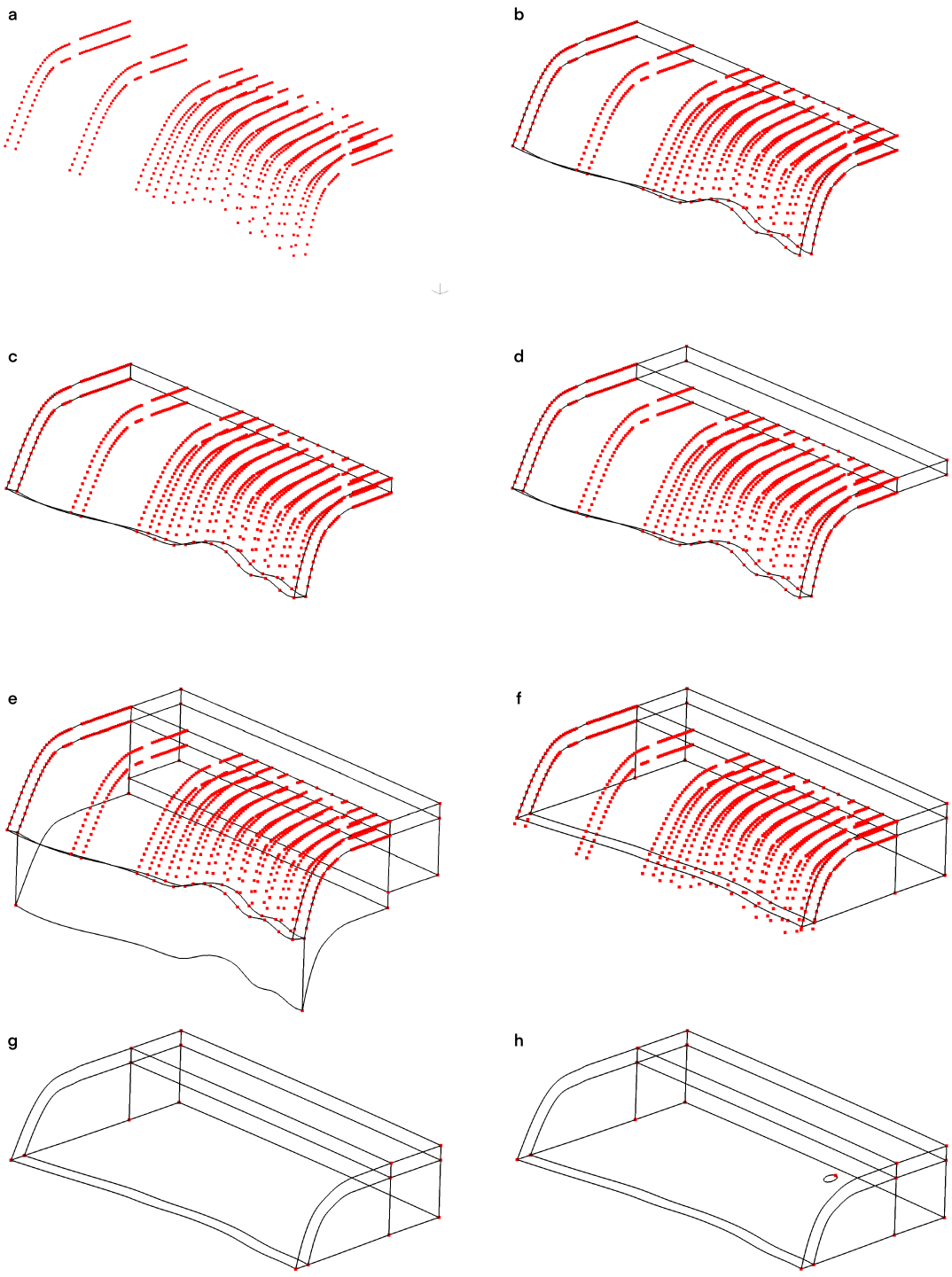

Figure 5: Process of constructing the subducting slab and sub slab mantle in Gmsh.

Points with an assigned depth of 3.2 km (representing the Pacific Plate east of the trench) were added to each cross-section to smoothen the transition between the Slab2 (Hayes et al., 2018) depth data and the edge of the model.
The thickness of the Pacific plate varies between 118 and 132 km along the Hikurangi margin and averages about 125 km (figure 3b, Hayes et al., 2018). Since the model slab is elastic, its thickness should not necessarily correspond to the lithosphere thickness of the Pacific plate but rather to its effective elastic thickness, which is around 60 km (Tesauro et al., 2012). Based on the effective elastic thickness, the slab was chosen to have a constant thickness of 60 km. To achieve this the base of the slab was created by copying each Slab2 data point and moving it 60 km downward perpendicular to the slab dip in that point (figure 3a, Hayes et al., 2018). The data points were converted to Cartesian coordinates. Then, the points were used to construct the slab volume in Gmsh (version 4.10.5, Geuzaine and Remacle, 2009) making use of the OpenCASCADE kernel. To do this, all points were put in a Gmsh file ordered by cross-section (figure 5a). Splines were drawn through the outer cross-sections on the top and bottom and through the first and last points of each cross-section on the top and bottom (figure 5b). These splines are the bounds of the top and bottom slab surfaces. The other cross-sections were included with the 'Using Point' option that comes with the OpenCASCADE kernel. The top and bottom surfaces were then connected with four side surfaces to create a volume (figure 5c). As the edge of the slab was too close to the trench this way, the edge was extruded 250 km in the positive x direction (figure 5d). To create the sub slab mantle, the bottom surface of the slab was extruded 300 km in negative z direction and then truncated at z=-298 km to ensure a straight bottom edge of the geometry (figures 5e and f). All unnecessary points were deleted, leaving the slab geometry shown in figure 5g. The asperity was added by including a cylinder in the geometry and using the BooleanIntersection function to leave only the circular surface within that cylinder that intersects with the top surface of the slab (figure 5h).

2.2.2 Australian plate

Moho depth varies between 20 and 35 km on the North Island and northern South Island of New Zealand (figure 6, data from Salmon et al., 2013 and Afonso et al., 2019). The modelled overriding plate represents both the crust and part of the lithospheric mantle and therefore has a thickness of 40 km. Additionally, the model geometry is set up so that the bottom of the overriding plate defines the end of the megathrust on the interface. Previous workers have defined ∼40 km depth as the deepest part where the downgoing and overriding plates are interseismically coupled at the Hikurangi margin (Wallace et al., 2004). A thickness of 40 km for the elastic overriding plate is also consistent with other 3D subduction zone models (D'Acquisto et al., 2023; Govers et al., 2018; Herman and Govers, 2020b; Herman et al., 2018) and lies within the range of a typical brittle-ductile transition (Abers et al., 2020). It is not likely that the process of subduction will significantly influence the topography (or vice versa) on a 40 year timescale so topography is not included to simplify the model.
The modelled overriding plate is based on two flat, rectangular surfaces at z=0 and z=-40 km, connected by side surfaces to form a volume (figure 7a). The surface at z=-40 km was extruded twice. First to the bottom of the geometry (z=-298 km) to form the mantle wedge and then to z=-80 km. Above depths of ∼80 km the subducting slab is not yet coupled to the mantle, which results in relatively cold, stationary material. This corner of the mantle wedge between the overriding plate and the slab is commonly referred to as the cold nose (Abers et al., 2020; Luo and Wang, 2021). At this point (figure 7b), the 'Australian' part of the model consisted of two volumes (overriding plate and mantle wedge) and the surface at 80 km depth (which will be used to construct the cold nose later). It was cut into shape using the bounds of the domain (based on the outer cross-sections used to define the slab) and the model trench (figures 7c and d). The trench consists of two line segments (thick black line in figure 4a) based on the Hikurangi trench as defined by Bird (2003) (grey line in figure 1). The trench is defined as a vertical boundary of the overriding plate to avoid an infinitesimally small taper, which may cause problems with meshing.

2.2.3 Combining the Pacific and Australian plates

The result of adding the slab and overriding plate geometries together is shown in figure 8a. The overriding plate, mantle wedge and cold nose surface intersect the slab and sub-slab, instead of terminating against the slab. With the BooleanFragments option, the overriding plate and mantle wedge were cut into shape while at the same time defining the top (at z=0 km) and bottom (at z=-40 km) of the megathrust on the slab (figure 8b). Figure 8b shows that where the overriding plate meets the slab, its thickness decreases gradually until it terminates at the trench. The minimum thickness of the overriding plate is 3.2 km at the easternmost part of the trench. The cold nose surface, which still intersected the slab at this point, was cut using the BooleanIntersection option so only the part inside of the slab remained. This smaller surface was extruded to z=-39 km, resulting in a volume diagonally cut in half by the slab with the top 1 km intersecting the overriding plate. Lastly, the BooleanDifference option was used to delete the parts of the volume overlapping with the slab and overriding plate. The cold nose is the remaining volume (figure 8c). An illustration of the resulting geometry is shown in figure 9.

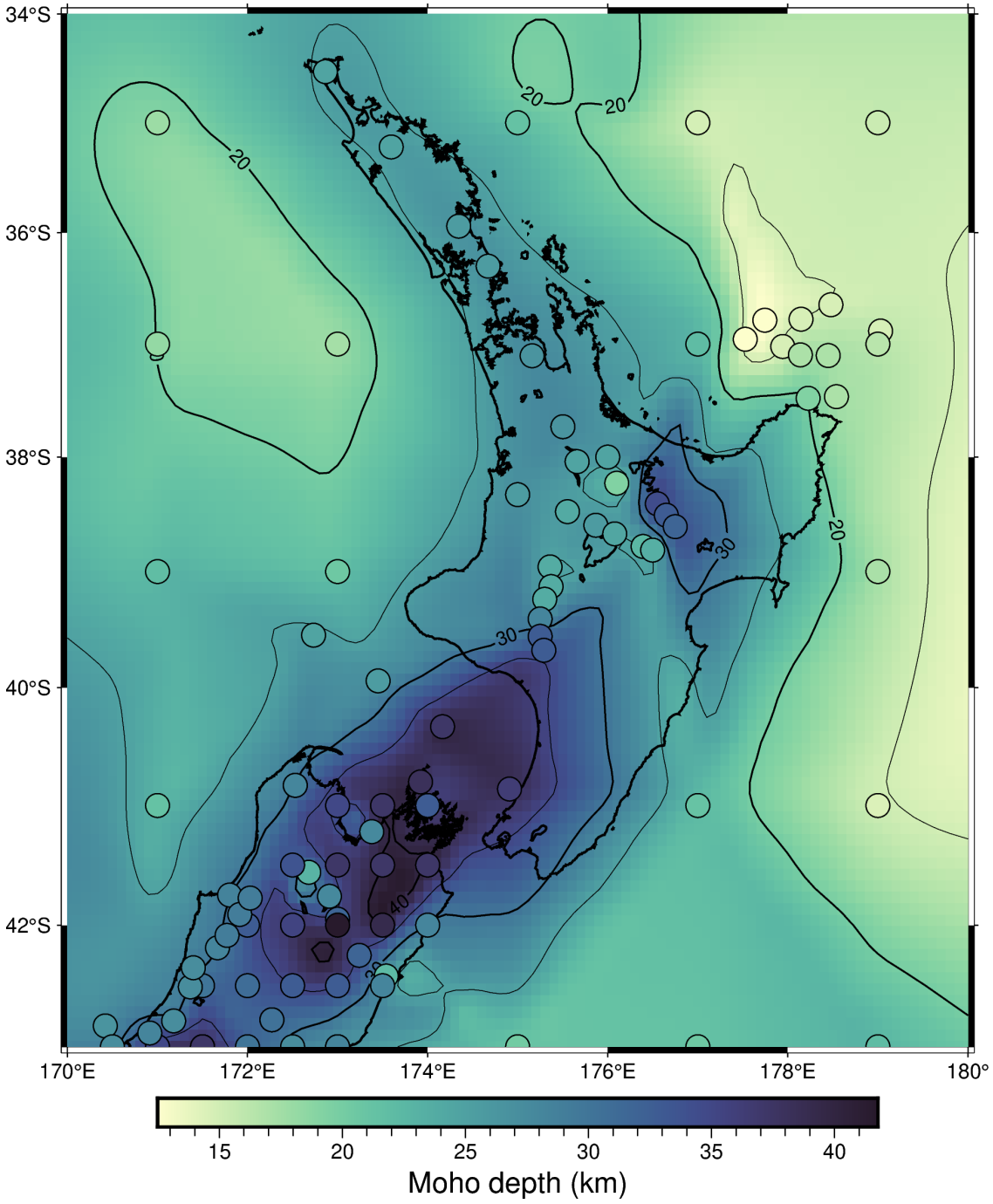

Figure 6: Interpolated crustal thickness of the North Island of New Zealand and its surroundings based on data from Salmon et al. (2013) for the continental portion and Afonso et al. (2019) to supplement data for the oceanic surroundings

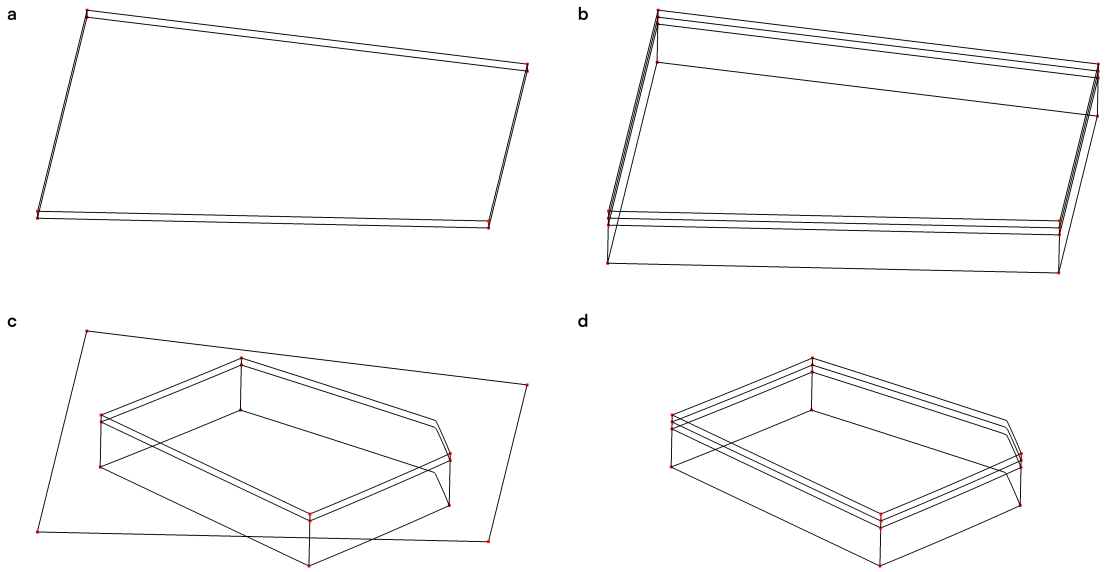

Figure 7: Process of constructing the overriding plate, cold nose and mantle wedge in Gmsh.

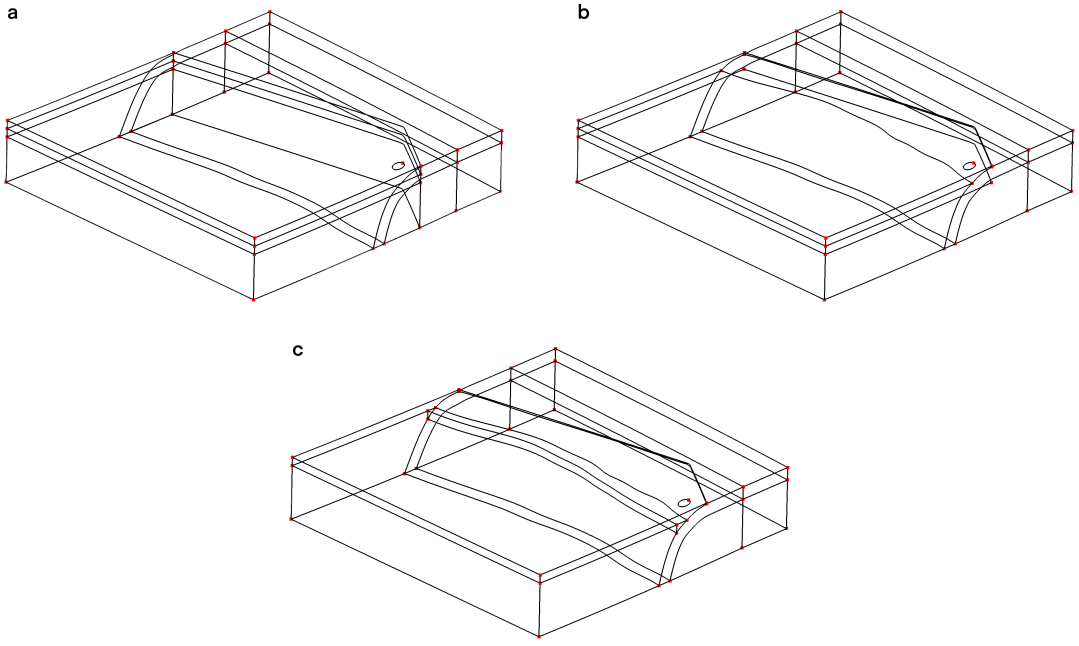

Figure 8: Process of combining the subducting slab and sub slab mantle with the overriding plate, cold nose and mantle wedge in Gmsh.

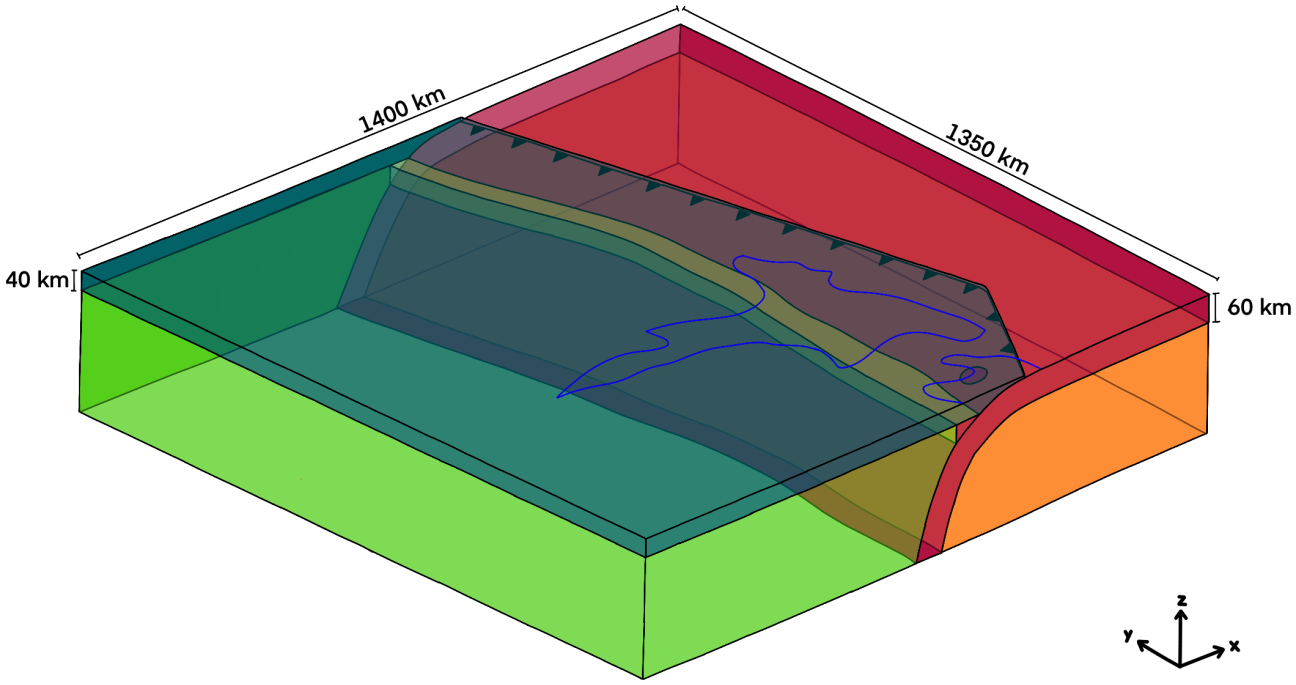

Figure 9: Illustration of the model geometry with the five different volumes: the slab in red, the sub-slab mantle in orange, the cold nose in yellow, the overriding plate in dark green and the mantle wedge in bright green. The coastline of New Zealand and the trench are projected on top of the model for clarity.

2.3 Mechanical properties

To simplify the model, it is divided into an elastic and a viscoelastic part. The top 40 km of the overriding plate, the subducting slab and the cold nose are chosen to be elastic, with a viscosity of 10^{30} Pa s. The mantle wedge beneath the elastic overriding plate and the sub-slab mantle are viscoelastic and have a viscosity of 10^{19} Pa s. Young's modulus is chosen to be 100 GPa and Poisson's ratio is 0.25. Both are uniform throughout the model. This corresponds to a Shear modulus of 40 GPa. The viscoelastic part of the model is chosen to have a Maxwell rheology, which means that the relaxation time of the model is about 8 years. These properties are based on other 3D subduction zone models with similar purposes and are consistent with PREM for the top 40 km (Dziewonski and Anderson, 1981; Govers et al., 2018; Herman and Govers, 2020b; Herman et al., 2018).

2.4 Boundary conditions

The boundary conditions are illustrated in figure 10. On the oceanic side of the slab, a horizontal velocity boundary condition of 43 mm/y was imposed at an angle of 41 degrees to the eastern edge of the slab. This was based on the direction and magnitude of the velocity of the Pacific Plate near Hawke's Bay (figure 1, DeMets et al., 1994; Nicol and Beavan, 2003). Hawke's Bay is located approximately at the center of the margin with plate velocity increasing northwards and decreasing southwards along the margin. Therefore, the plate velocity at Hawke's Bay was chosen as an average for the entire margin. The slab moves in the negative x and y directions. The easternmost bottom edge of the sub-slab mantle is not allowed to move at all. Where the slab leaves the bottom of the model at 298 km depth, the same velocity boundary condition as on the oceanic side was imposed, but the x-component was rotated to be parallel to the dip of the slab there. The rotation adds a vertical component to the applied velocity, making sure the slab moves downward instead of just horizontally through the domain. The western side of the domain is not allowed to move in any direction. Therefore, displacement will approach zero towards this 'backstop'. Backstop location can have a significant influence on horizontal surface displacement in the model. When the backstop is too close to the region of interest, horizontal surface displacements decrease inaccurately away from the trench. In this specific model, the backstop will not influence model results significantly, as horizontal surface displacements are already close to 0 west of the

Taupo Volcanic Zone (figure 2; Beavan et al., 2016). The sides of the model are left open to avoid edge effects, especially since the southern edge of the model is close to the research area. The bottom interface between the slab and sub-slab mantle consists of slippery nodes (Melosh and Williams Jr, 1989). This allows the slab to slide freely along this interface. The top interface can be entirely slippery, but it is also possible to partly lock the megathrust. This is done by imposing large (10^{20} Pa) differential Winkler forces on part of the fault, an asperity. The asperity has a diameter of 50 km and can be placed anywhere on the megathrust. When the asperity is locked, there can be no slip on that surface. Everything outside the asperity is allowed to slip without resistance, but the asperity will limit motion around it. Therefore, the area surrounding the asperity will not slip at the convergence rate imposed on the sides of the model (Herman and Govers, 2020a; Herman et al., 2018). For the purpose of testing the model geometry and boundary conditions, the asperity is placed in the southern part of the domain, with its center at y=-310 km.

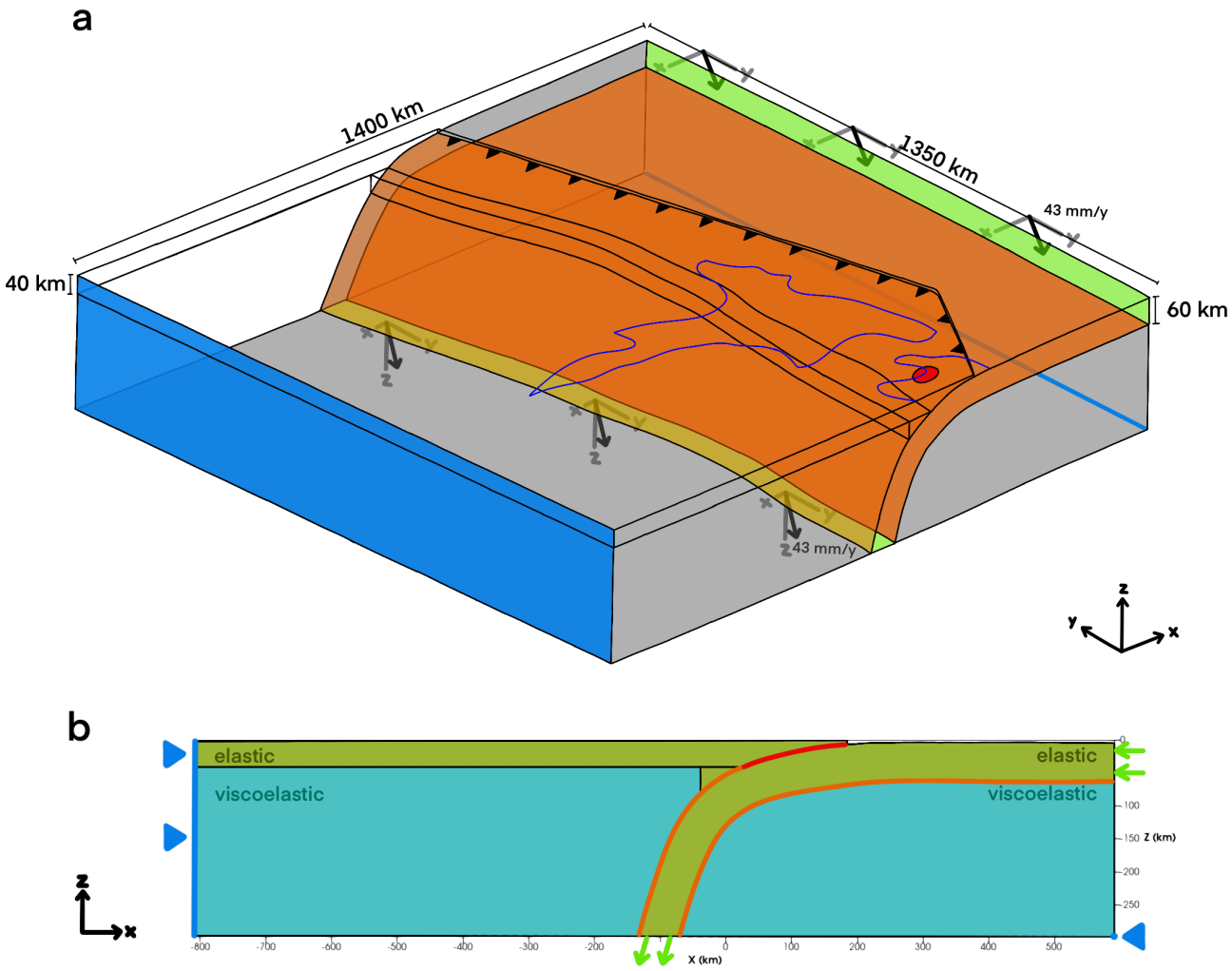

Figure 10: The model's boundary conditions, a) shows the whole model with the coastline of New Zealand and the trench projected on top. The arrows show the direction and magnitude of the imposed velocity on the green colored edges of the model.The surfaces with slippery nodes are orange. The red circle has the possibility to be locked but is slippery too if not. The blue surfaces and line show where a displacement boundary condition is imposed on the model's edges. In b) the boundary conditions are shown again but now as a cross-section through the model. Green parts are elastic while blue parts are viscoelastic. The orange lines show surfaces where slippery nodes were added. The red line is the megathrust, with slippery nodes as well but also the possibility to lock part of this surface. The green arrows show the direction of the velocities imposed and the blue triangles show the displacement boundary condition.

2.5 Numerical model

Displacement along the Hikurangi margin is modelled using the 3D finite element code GTECTON (version 2023.dev, Govers and Wortel, 2005). GTECTON uses PETSc (version 3.17.2, Balay et al., 1997, 2022a, 2022b) and OpenMPI (version 4.1.5UCX, Gabriel et al., 2004) to solve the mechanical equilibrium equations. The used mesh (generated using Gmsh version 4.10.5, Geuzaine and Remacle, 2009) has the highest resolution close to the asperity. The remaining interface from the trench down to the coupling of the downgoing plate and mantle wedge (at 80 km) also has a relatively fine mesh. The remaining mesh has a lower resolution to save on computation time. Based on the prescribed Young's modulus of 100 GPa and viscosity of 10^{19} Pa s, the Maxwell relaxation time of the mantle wedge and sub-slab mantle is ∼8 years. The model runs for 40 years (5 relaxation times, to make sure that full viscous relaxation is reached) with a time step of 0.5 years.

3 Test results

The model design is validated using two tests. One is a model where the subducting slab is stably sliding without resistance. In the other model, a circular patch on the megathrust, with a diameter of 50 km, is locked. This means that that patch is fully coupled to the overriding plate above, simulating the accumulation of slip deficit that may cause an earthquake. Away from this so-called asperity, the slab is expected to move with the imposed velocity. In this section, both models are shown and compared after 40 years of displacement at 43 mm/y.

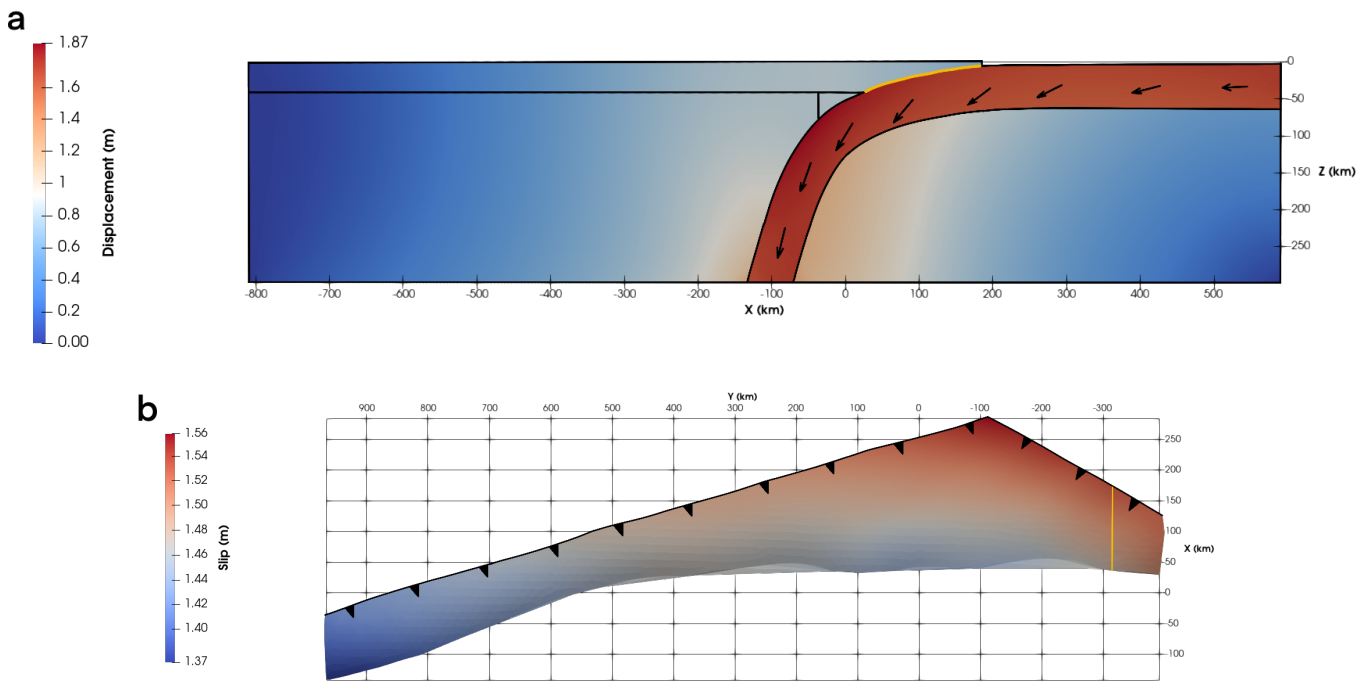

Figure 11: a) Cross-section through the model without locking, showing displacement in meters after 40 years and b) top view of slip on the megathrust in meters after 40 years of displacement at 43 mm/y without locking. The yellow lines in a) and b) are at the same location in both figures.

3.1 Displacement and slip

After 40 years, 1.72 m of slab-parallel displacement is expected in the straight segments of the free-slipping model. Where the slab bends, displacement is expected to deviate from the 1.72 m, with more displacement above and less displacement below the mid-plane due to deformation related to the bending of the slab. The slab's top and bottom surfaces consist entirely of slippery nodes (i.e. the slab is able to slide independently of its surroundings). Consequently, there should be no displacement outside the slab.

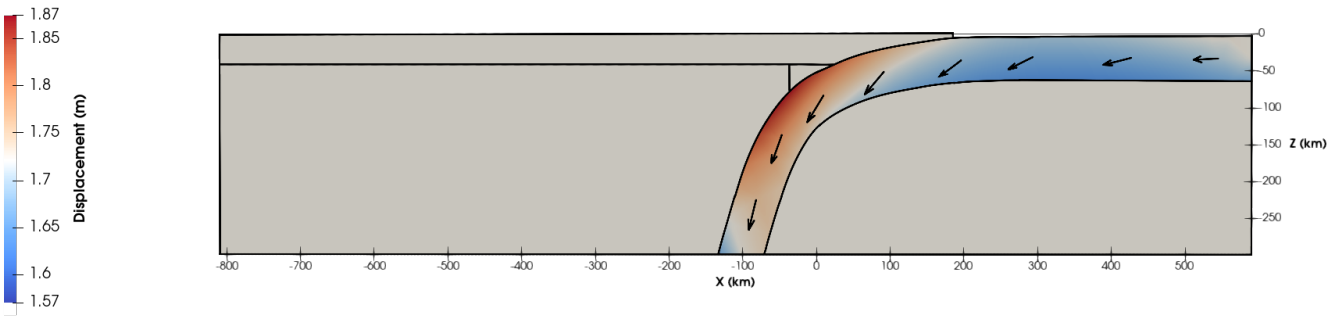

Figure 12: Cross-section through the model without locking, showing displacement in meters after 40 years with a different color scale highlighting the differences in displacement within the slab.

Figure 11a shows the displacement magnitude in a cross-section at y=-310 km through the free-slipping model. Figure 11b shows the location of the cross-section on the megathrust. Displacement is concentrated in the slab, but not zero outside it. Displacement outside the slab is mainly vertical. Figure 11a shows that displacement is not parallel to the slab. The vertical component of the displacement increases too fast, causing the slab to sink. The overriding plate sinks with it. The sinking leads to vertical displacement in the sub-slab mantle, which is relatively weak due to its lower viscosity and a lack of buoyancy forces resisting the sinking.The displacement not being slab-parallel is a consequence of a lack of control on the drive of the slab, as it is driven only by the velocity boundary conditions where the slab enters at the oceanic side and leaves at the bottom of the domain. Slip on the megathrust is impacted as well, which is to be expected as it only involves slab parallel motion. Figure 11b shows that slip is not spatially constant. More slip indicates a smaller slab-perpendicular component of displacement. This shows that along dip, displacement is more slab-parallel closer to the trench, which is valid as the trench is closest to the horizontal drive of the slab. Slip also varies along strike and is smallest around y=700-950 km. This is possibly related to the shape of the megathrust. The highest slip is achieved where the megathrust is the most flat. In the north, the megathrust is relatively steep and thus there is less slip. The southernmost part of the slab is also steep, but the megathrust is less steep than in the northern part of the domain. From the contrast in displacement magnitude between the slab and its surroundings it can be concluded that the slippery nodes are mostly functional, but not perfect. Because the model geometry is still in a testing stage, a relatively coarse mesh was used. Representing the irregular slab surfaces with a coarse mesh causes the mesh to be 'bumpy' instead of smooth, hindering the slippery nodes. This causes part of the slab displacement to be transferred to the mantle and overriding plate.

Figure 12 highlights displacement within the slab and shows that the expected pattern of displacement that was described before is not achieved. In the horizontal part of the slab, there is less than 1.72 m of displacement. There is 1.87 m of displacement above the mid-plane where the slab bends. Below the mid-plane, there is approximately 1.75 m of displacement. This may also be caused by the displacement not being parallel to the slab dip. The displacement vectors in the slab start bending before the slab geometry starts bending, which results in the mid-plane (of the bend described by the displacement vectors) being mostly outside the slab. At the bottom of the model there is around 1.72 m of displacement, with exception of a corner where there is less displacement. This is caused by GTECTON not allowing a velocity boundary condition on an edge with slippery nodes. Therefore, the nodes of that edge have no boundary condition applied to it and thus have lower velocity than the other nodes on the bottom surface.

Figure 13 is a cross-section at the same location as the one in figure 11a, but through the model with locking. Similar to the free-slipping model, displacement is concentrated in the slab and decreases away from it. At the location of the asperity, displacement is increased in the overriding plate and decreased in the slab. Their similar amounts of displacement indicate that they are coupled. One of the objectives of this project is mechanically continuous locking on the megathrust. Figures 14a and 14b show a comparison between slip on the megathrust without locking and with locking. In the locking model, there is zero slip inside the asperity and slip is reduced around it. This is similar to the results of Herman et al. (2018), from which it can be assumed that locking the asperity with high differential Winkler forces works. Away from the asperity, slip gradually increases but it never reaches the level of slip of the free-slipping model.

To isolate the effect of locking part of the megathrust, the difference between the two models is shown in figure 15. As expected from Govers et al. (2018), locking results in shortening of the overriding plate and shear deformation of the slab near the asperity. The extra displacement in the cold nose and mantle wedge was not expected, but can again be explained by the lack of buoyancy forces in the model. The vertical component of the overriding plate's displacement pushes down on the cold nose and mantle wedge without resistance.

These results show that displacement is not slab-parallel, which causes deformation in other parts of the model. This needs to be corrected in future model iterations. The results from locking the asperity are as expected, especially on the megathrust.

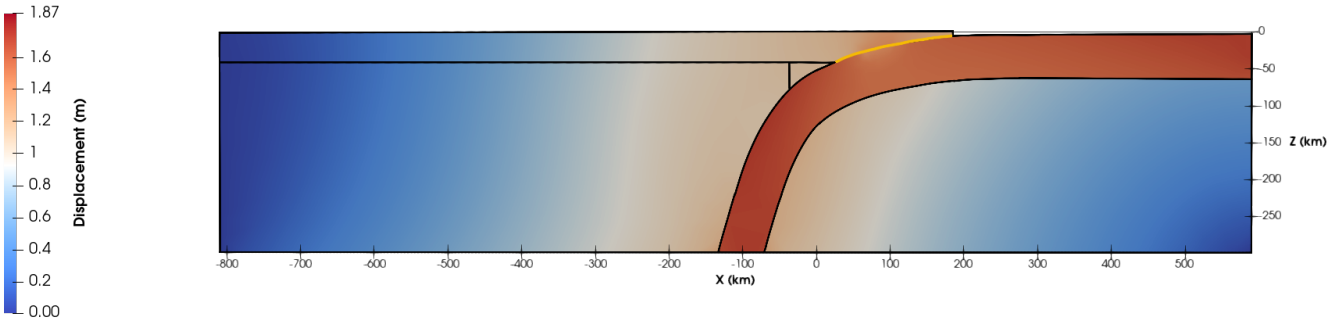

Figure 13: Cross-section through the model with locking, showing displacement in meters after 40 years.

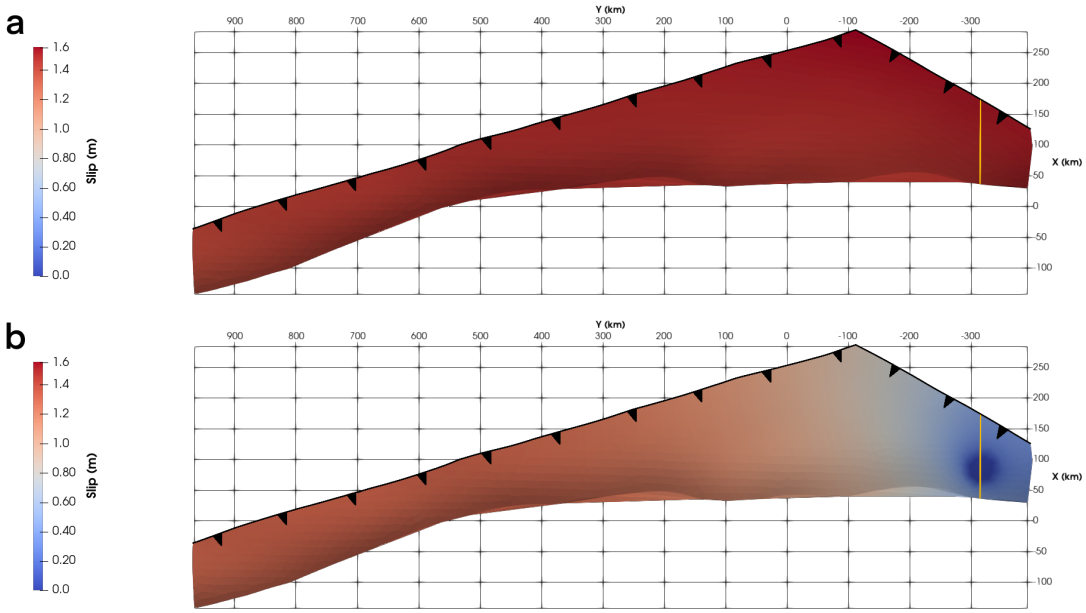

Figure 14: a) Top view of slip on the megathrust in meters after 40 years of displacement at 43 mm/y with a) a free-slipping interface and b) a locked asperity on the megathrust. Figure 14a is the same as figure 11b, with an adjusted scale for clear comparison.

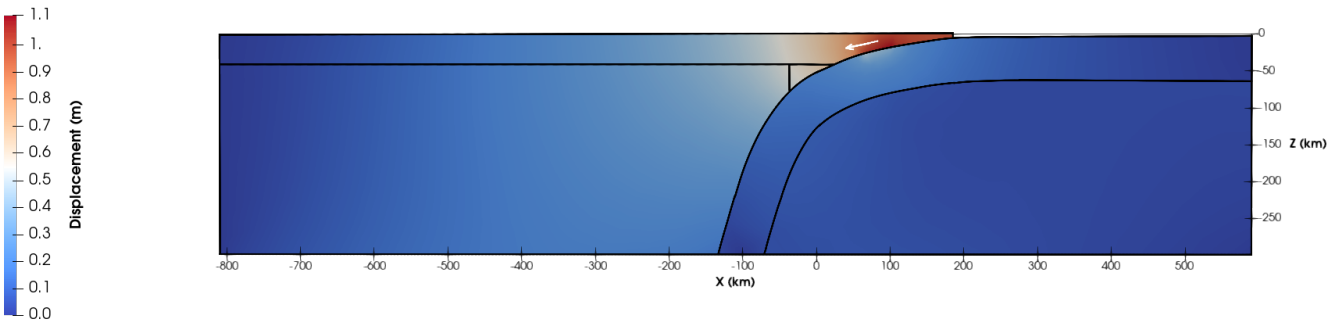

Figure 15: Difference in displacement in meters after 40 years between the model with and the model without locking.

3.2 Shear traction

In the previous section, it was already stated that while the slippery nodes are functional, they are not perfect. To further confirm this statement, shear traction on the slab's top surface was evaluated. There should be zero resolved traction on the free-slipping surface if the slippery nodes work perfectly (Melosh and Williams Jr, 1989). Inside the asperity a pattern of shear traction that is high along the edge and decreases towards the middle is expected. Directly outside the asperity, everything slides stably and shear traction should be zero again (Herman et al., 2018). Shear tractions on the interface are calculated using the components σ_{ij} from the Cauchy stress tensor and normals $\hat{\mathbf{n}}$ on the surface of the subducting slab. Figure 16 indeed suggests that the model should be improved: the accumulated shear tractions are relatively small (compared to shear traction inside the asperity in figure 17) but not zero. The same relatively small shear tractions are present in the model with the locked asperity, shown in figure 17. Presumably these non-zero shear tractions are again caused by the model's mesh being too coarse. The interface of the asperity model accumulates the most shear stress inside the asperity (up to 430 MPa). The expected pattern is not visible however, and, more importantly, there is not zero shear traction directly outside the asperity, which is unexpected. This inconsistency can be explained by the way the shear tractions were calculated, as the components of the stress tensor are calculated per element (so concentrated in its center), while normal vectors are calculated on the nodes (at the corners of the element). Combining element en node data to calculate shear stress on the plane might skew the location of the shear stress accumulation and assign it to an element outside the asperity because it shares a node with an element inside the asperity. These shear stress calculations show that the basic features of the model are present. However, due to a relatively low mesh resolution some stresses build up outside of the asperity.

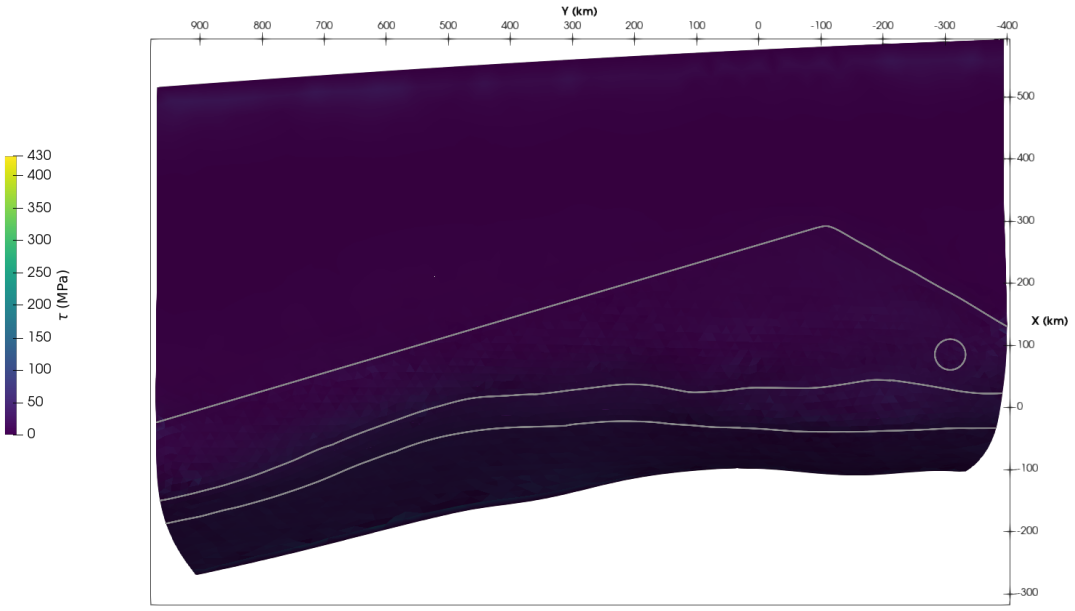

Figure 16: Top view of shear stress on the slab's top surfaces of the stably sliding model. The lines show the different surfaces that were defined. Scale is the same as figure 17.

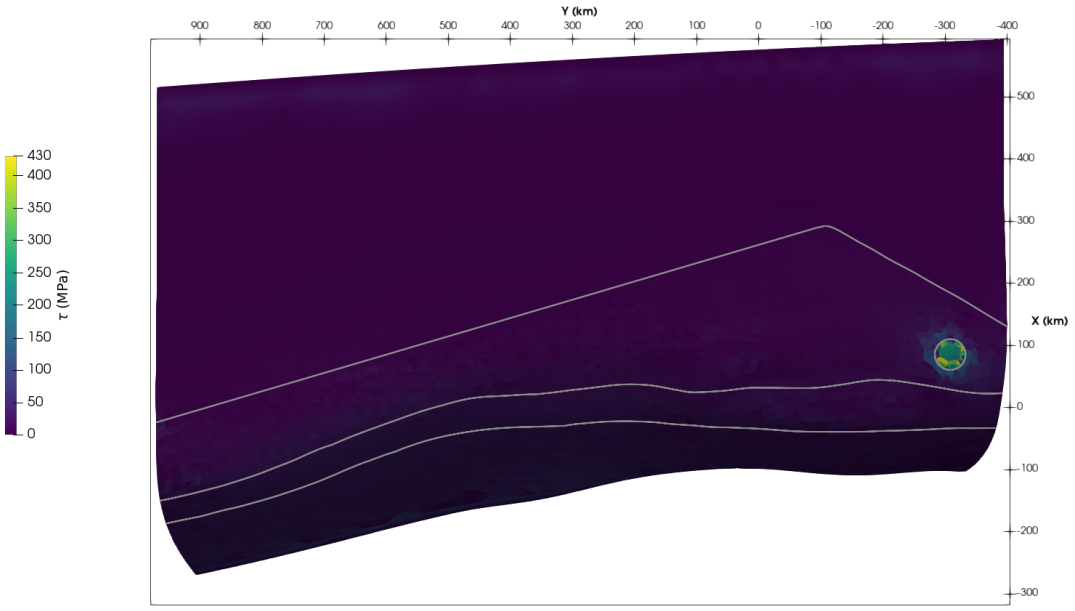

Figure 17: Top view of shear stress on the slab's top surfaces of the model with a locked asperity. The lines show the different surfaces that were defined, the asperity is the circular feature around x = 90 km and y = -310 km. Scale is the same as figure 16.

3.3 Horizontal surface velocities

To test the functionality of the locking the horizontal surface velocities produced by the model are compared to GPS velocities within the domain. Since the asperity is relatively small and the model is very simplified at this stage a great fit is not expected. Additionally, the model only accounts for horizontal surface velocities due to locking while, as elaborated upon in the introduction of this work, surface velocities in New Zealand (specifically the northern North Island) are influenced by back arc extension in

the TVZ as well. The horizontal surface velocities on the overriding plate (figure 18) again show how the overriding plate moves along with the subducting slab when they are partly mechanically coupled. It also shows that this coupling influences not just the part of the overriding plate directly overlying the locked portion of the slab. Significant velocities of 10 mm/y (whereas the slab has a velocity of 43 mm/y) are seen 500 km away from the center of the asperity (at y = -310 km), meaning that locking a patch, with a diameter of 50 km, beneath the northern South Island, influences horizontal surface velocities on the northern North Island. Comparing figure 18 to figure 2 shows that the single locked asperity in the model already produces horizontal surface velocities similar to GPS velocities on the southern North Island and northern South Island. As expected, the northern North Island is not approximated at all. From figure 18 it is evident that the overriding plate is coupled to the slab and that this coupling is mechanically continuous, as was intended.

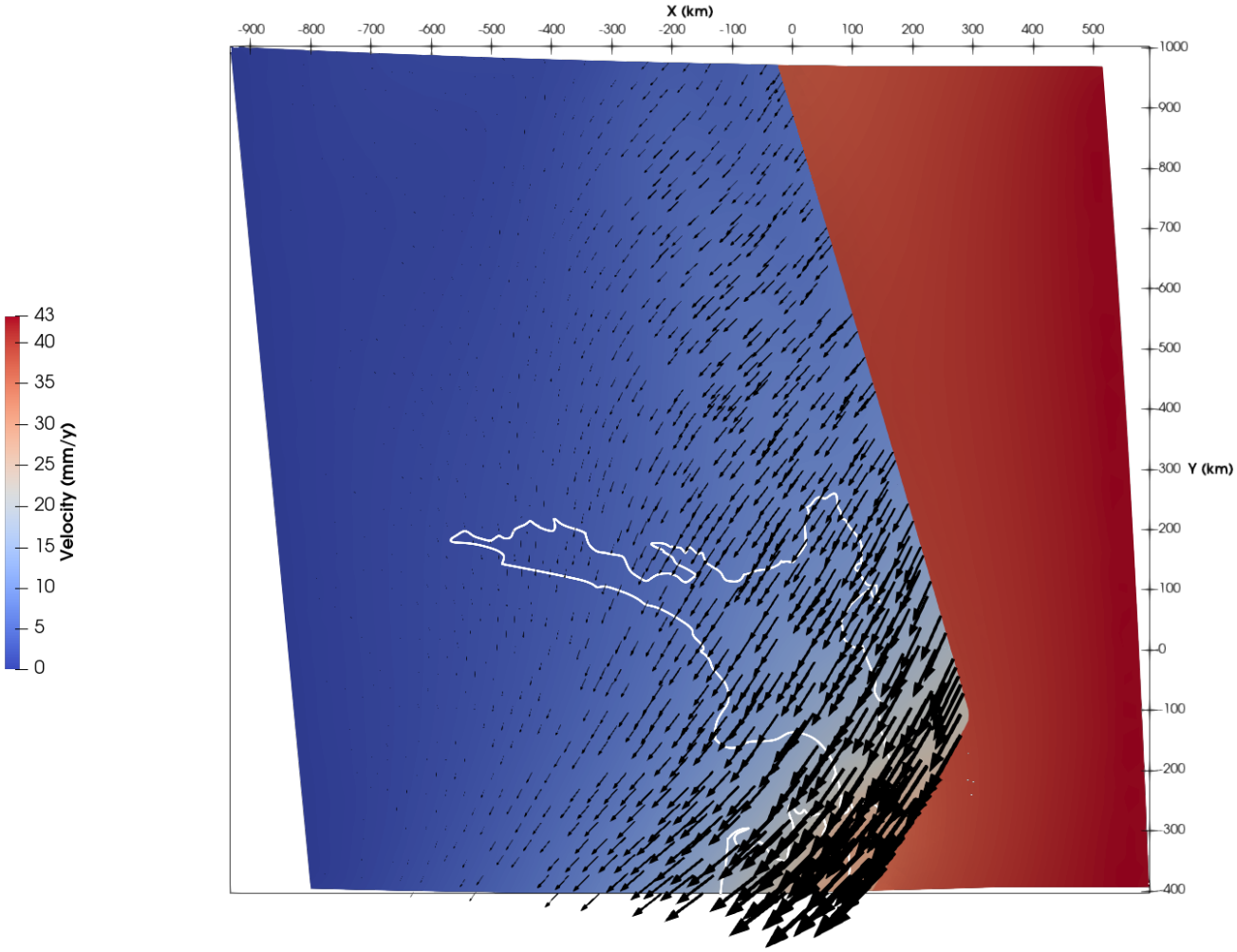

Figure 18: Top view of horizontal surface velocity in the model. Coloring shows magnitude of the velocity and arrows show direction on the overriding plate only.

4 Discussion

4.1 Room for future model improvement

The two main flaws of the model are the slippery nodes not working perfectly and slab displacement not being slab-parallel. It is expected that the problem with the slippery nodes can be solved by making the model's mesh finer. The direction in which each slippery node can slip is determined by Euler angle rotations that rotate a local coordinate system (x-axis parallel to the slab surface at a specific node) into the global coordinate system (x-axis parallel to the top of the overriding plate). In the coarse mesh used in this model iteration the nodes on the slab surfaces are too far apart. On a highly variable slab surface this

causes Euler angle calculations to be inaccurate in between nodes. The local coordinate system then is not slab-parallel and the slip direction is off. A finer mesh and thus more nodes on the surfaces will represent the highly variable surfaces better. As a result, the slab will be able to slide without resistance (and thus without shear traction accumulation), as was intended. The slab displacement can be made parallel to the slab by controlling the slab's driving velocity further than just at the edges of the model domain. This can be done by using faulted nodes to impose the slab velocity of 43 mm/y on the slab's top and bottom surfaces (apart from the megathrust) (D'Acquisto et al., 2023; Melosh and Raefsky, 1981).

4.2 Simplification of model geometry

While constructing the model geometry some simplifications had to be made. The subducting slab itself is relatively complex due to its along strike and along dip variation, but more cross-sections than the thirteen that were used could be added (figure 4b). Especially in the south the shape of the slab varies significantly between cross-sections and their error margins do not overlap. Less space between cross-sections may be useful to rely less on interpolation. The southern boundary was put at 42 °S because the shape of the slab changes significantly from there as it transitions into the Alpine fault (figure 4a and b). The downside of this approach is that the edge of the model is close to the research area, which introduces edge effects. To counteract those, no boundary conditions were imposed on the edges so material is free to flow in and out of the model. Figures 11b and 13b show that the edge effects indeed seem minimal as slip is continuous on the edges of the megathrust. Nonetheless, the southern boundary might need a boundary condition that simulates the reality better. The two continental plateaus (Chatham Rise and Challenger Plateau) that cause subduction to cease (Beavan et al., 2002; Wallace et al., 2009) introduce a resisting force to the model that should be implemented in future iterations. The overriding plate was given a constant thickness of 40 km, while the crustal thickness varies between 20 and 40 km within the domain. This does not mean that in future model iterations the overriding plate should be made thinner, as was explained in section 2.2.2. Figure 6 shows that New Zealand is essentially a thin strip with thicker (continental) crust surrounded by thinner (oceanic) crust. The crustal lithosphere of New Zealand itself is weaker than its surroundings (Tesauro et al., 2012). Changing the material strength of the overriding plate so that the part of the west coast of New Zealand is stronger than the part beneath New Zealand would therefore be a relevant addition to the model.

4.3 Surface velocities

Future research should include confirming whether it is possible to account for surface velocities on the northern North Island using locking or they are caused by a different mechanism. A proposed mechanism capable of causing these differently oriented GPS velocities is the back-arc extension in the TVZ, as its direction is opposite to the convergence along the Hikurangi margin (Wallace et al., 2009). The TVZ is not included in this model, because this study focuses on the influence of interseismic locking only. Including an extensional fault in the model could lead to new insights, if it is indeed not possible to approximate the velocity field with locking only. It is important to note that reproducing the locking pattern with a sharp transition proposed by Wallace et al. (2004) and Wallace et al. (2012) is not possible when the binary locking method is used. Binary locking produces asperities that are mechanically continuous with their surroundings. Figure 18 shows that surface velocities on the overriding plate are affected several hundreds of kilometers away from an asperity. The locking pattern of Wallace et al. (2012) is, therefore, not likely to be reproduced regardless of its validity. Furthermore, it is possible that the same surface velocity pattern can be produced using several smaller asperities instead of one large asperity, because the area surrounding an asperity accumulates a slip deficit even though it is not coupled to the overriding plate. A more systematic approach may be needed to determine possible locking patterns.

4.4 Masking of slip rate deficit

According to Wallace et al. (2010), the sharp transition in the locking pattern from Wallace et al. (2004) can be explained by the contrasting characteristics between the northern and southern sections of the Hikurangi margin. Rather than using some of these characteristics, like the extension in the TVZ as well as shallow slow slip events in the northern part of the margin, as a reason why the transition is there, they could be seen as factors that mask the accumulation of slip deficit. The opposing directions of motion at the Hikurangi margin and TVZ (Wallace et al., 2009) could produce a combined motion in a different direction on the surface, without that meaning that there is no locking at greater depths. This locking at large depths can then cause the updip part of the megathrust to accumulate slip deficit as well, due to the so-called stress shadow (Almeida et al., 2018). This would imply that the earthquake risk on the northern North Island is larger than expected. Meade (2022) showed that interseismic surface velocities near faults may not approximate the long-term slip on these faults, and that tectonic processes at these fault could be masked by processes related to the earthquake cycle. Slow slip events are one of these processes, whether they happen right before an earthquake (preslip), right after (afterslip), or somewhere in between (interseismic slip) (Schwartz and Rokosky, 2007).

5 Conclusion

The aim of this project was to construct a 3D model geometry based on the Hikurangi subduction zone. The geometry was tested by comparing two models: one where the subducting slab is freely slipping and one where a circular feature on the megathrust is coupled to the overriding plate. These tests showed that locking results in shortening of the overriding plate and mechanically continuous slip on the megathrust. Locking of the asperity influences horizontal surface velocities 500 km away from its center, dragging the overriding plate along with the subducting slab. Displacement and shear traction in the free-slipping model showed that a finer mesh and more control on the drive of the slab is needed to produce more realistic results. However, even with the limited features of the model during this testing stage it can be concluded from the locking results that the model geometry is promising and ready to be used in the next phase of this project.

6 Acknowledgements

I want to thank Rob Govers, for his guidance during this project. Next, I want to thank Lukas van de Wiel for helping me with technical difficulties. I want to thank Celine Marsman for helping me understand Euler rotations in 3D, Weilun Qin for the helpful discussions about Gmsh and slippery nodes and Sietse Vos and Saskia Vos for proofreading my work. Lastly, I want to thank Cedric Thieulot for assessing this thesis. Maps were made using PyGMT (version 0.10.0, Tian et al., 2023). Figures related to the model geometry were made using Gmsh (Geuzaine and Remacle, 2009) and Procreate. The results were presented with ParaView (Ahrens et al., 2005).

References

Abers, G. A., van Keken, P. E., & Wilson, C. R. (2020). Deep decoupling in subduction zones: Observations and temperature limits. *Geosphere*, *16*(6), 1408–1424.

Afonso, J. C., Salajegheh, F., Szwillus, W., Ebbing, J., & Gaina, C. (2019). A global reference model of the lithosphere and upper mantle from joint inversion and analysis of multiple data sets. *Geophysical Journal International*, *217*(3), 1602–1628.

Ahrens, J., Geveci, B., Law, C., Hansen, C., & Johnson, C. (2005). Paraview: An end-user tool for large-data visualization. *The visualization handbook*, *717*, 50038–1.

Almeida, R., Lindsey, E. O., Bradley, K., Hubbard, J., Mallick, R., & Hill, E. M. (2018). Can the updip limit of frictional locking on megathrusts be detected geodetically? quantifying the effect of stress shadows on near-trench coupling. *Geophysical Research Letters*, *45*(10), 4754–4763.

Balay, S., Abhyankar, S., Adams, M. F., Benson, S., Brown, J., Brune, P., Buschelman, K., Constantinescu, E., Dalcin, L., Dener, A., Eijkhout, V., Gropp, W. D., Hapla, V., Isaac, T., Jolivet, P., Karpeev, D., Kaushik, D., Knepley, M. G., Kong, F., ... Zhang, J. (2022b). *PETSc/TAO users manual* (tech. rep. No. ANL-21/39 - Revision 3.17). Argonne National Laboratory.

Balay, S., Abhyankar, S., Adams, M. F., Benson, S., Brown, J., Brune, P., Buschelman, K., Constantinescu, E. M., Dalcin, L., Dener, A., Eijkhout, V., Gropp, W. D., Hapla, V., Isaac, T., Jolivet, P., Karpeev, D., Kaushik, D., Knepley, M. G., Kong, F., ... Zhang, J. (2022a). PETSc Web page. https://petsc.org/

Balay, S., Gropp, W. D., McInnes, L. C., & Smith, B. F. (1997). Efficient management of parallelism in object oriented numerical software libraries. In E. Arge, A. Bruaset, & H. Langtangen (Eds.), *Modern software tools in scientific computing* (pp. 163–202). Birkhäuser Press.

Barker, D. H., Sutherland, R., Henrys, S., & Bannister, S. (2009). Geometry of the hikurangi subduction thrust and upper plate, north island, new zealand. *Geochemistry, Geophysics, Geosystems*, *10*(2).

Beavan, J., Tregoning, P., Bevis, M., Kato, T., & Meertens, C. (2002). Motion and rigidity of the pacific plate and implications for plate boundary deformation. *Journal of Geophysical Research: Solid Earth*, *107*(B10), ETG–19.

Beavan, J., & Darby, D. (2005). Fault slip in the 1855 wairarapa earthquake based on new and reassessed vertical motion observations: Did slip occur on the subduction interface. *The 1855 Wairarapa Earthquake Symposium*, *150*, 31–41.

Beavan, J., Wallace, L. M., Palmer, N., Denys, P., Ellis, S., Fournier, N., Hreinsdottir, S., Pearson, C., & Denham, M. (2016). New zealand gps velocity field: 1995–2013. *New Zealand Journal of Geology and Geophysics*, *59*(1), 5–14.

Bird, P. (2003). An updated digital model of plate boundaries. *Geochemistry, Geophysics, Geosystems*, *4*(3).

Blewitt, G., Hammond, W., & Kreemer, C. (2018). Harnessing the gps data explosion for interdisciplinary science. *Eos*, *99*.

Blewitt, G., Kreemer, C., Hammond, W. C., & Gazeaux, J. (2016). Midas robust trend estimator for accurate gps station velocities without step detection. *Journal of Geophysical Research: Solid Earth*, *121*(3), 2054–2068.

Calhaem, I. (1973). Asymmetric spreading from a volcanic arc to an active continental margin.

Clark, K., Hayward, B. W., Cochran, U. A., Wallace, L. M., Power, W. L., & Sabaa, A. T. (2015). Evidence for past subduction earthquakes at a plate boundary with widespread upper plate faulting: Southern hikurangi margin, new zealand. *Bulletin of the Seismological Society of America*, *105*(3), 1661–1690.

Clark, K., Howarth, J., Litchfield, N., Cochran, U., Turnbull, J., Dowling, L., Howell, A., Berryman, K., & Wolfe, F. (2019). Geological evidence for past large earthquakes and tsunamis along the hikurangi subduction margin, new zealand. *Marine Geology*, *412*, 139–172.

D'Acquisto, M., Herman, M., Riva, R., & Govers, R. (2023). Can plate bending explain the observed faster landward motion of lateral regions of the subduction zone after major megathrust earthquakes? *Journal of Geophysical Research: Solid Earth*, *128*(3), e2022JB025431.

Darby, D., & Beavan, J. (2001). Evidence from gps measurements for contemporary interplate coupling on the southern hikurangi subduction thrust and for partitioning of strain in the upper plate. *Journal of Geophysical Research: Solid Earth*, *106*(B12), 30881–30891.

Davy, B., & Wood, R. (1994). Gravity and magnetic modelling of the hikurangi plateau. *Marine geology*, *118*(1-2), 139–151.

DeMets, C., Gordon, R. G., & Argus, D. F. (2010). Geologically current plate motions. *Geophysical journal international*, *181*(1), 1–80.

DeMets, C., Gordon, R. G., Argus, D. F., & Stein, S. (1994). Effect of recent revisions to the geomagnetic reversal time scale on estimates of current plate motions. *Geophysical research letters*, *21*(20), 2191–2194.

Doser, D. I., & Webb, T. H. (2003). Source parameters of large historical (1917–1961) earthquakes, north island, new zealand. *Geophysical journal international*, *152*(3), 795–832.

Dragert, H., Wang, K., & James, T. S. (2001). A silent slip event on the deeper cascadia subduction interface. *Science*, *292*(5521), 1525–1528.

Dziewonski, A. M., & Anderson, D. L. (1981). Preliminary reference earth model. *Physics of the earth and planetary interiors*, *25*(4), 297–356.

Furlong, K. P., & Herman, M. (2017). Reconciling the deformational dichotomy of the 2016 mw 7.8 kaikoura new zealand earthquake. *Geophysical Research Letters*, *44*(13), 6788–6791.

Gabriel, E., Fagg, G. E., Bosilca, G., Angskun, T., Dongarra, J. J., Squyres, J. M., Sahay, V., Kambadur, P., Barrett, B., Lumsdaine, A., Castain, R. H., Daniel, D. J., Graham, R. L., & Woodall, T. S. (2004). Open MPI: Goals, concept, and design of a next generation MPI implementation. *Proceedings, 11th European PVM/MPI Users' Group Meeting*, 97–104.

Geuzaine, C., & Remacle, J.-F. (2009). Gmsh: A 3-d finite element mesh generator with built-in pre-and post-processing facilities. *International journal for numerical methods in engineering*, *79*(11), 1309–1331.

Govers, R., Furlong, K., Van de Wiel, L., Herman, M., & Broerse, T. (2018). The geodetic signature of the earthquake cycle at subduction zones: Model constraints on the deep processes. *Reviews of Geophysics*, *56*(1), 6–49.

Govers, R., & Wortel, M. (2005). Lithosphere tearing at step faults: Response to edges of subduction zones. *Earth and Planetary Science Letters*, *236*(1-2), 505–523.

Hayes, G. P., Moore, G. L., Portner, D. E., Hearne, M., Flamme, H., Furtney, M., & Smoczyk, G. M. (2018). Slab2, a comprehensive subduction zone geometry model. *Science*, *362*(6410), 58–61.

Herman, M., Furlong, K., & Govers, R. (2018). The accumulation of slip deficit in subduction zones in the absence of mechanical coupling: Implications for the behavior of megathrust earthquakes. *Journal of Geophysical Research: Solid Earth*, *123*(9), 8260–8278.

Herman, M., & Govers, R. (2020a). Locating fully locked asperities along the south america subduction megathrust: A new physical interseismic inversion approach in a bayesian framework. *Geochemistry, Geophysics, Geosystems*, *21*(8), e2020GC009063.

Herman, M., & Govers, R. (2020b). Stress evolution during the megathrust earthquake cycle and its role in triggering extensional deformation in subduction zones. *Earth and Planetary Science Letters*, *544*, 116379.

Hirose, H., Hirahara, K., Kimata, F., Fujii, N., & Miyazaki, S. (1999). A slow thrust slip event following the two 1996 hyuganada earthquakes beneath the bungo channel, southwest japan. *Geophysical Research Letters*, *26*(21), 3237–3240.

Luo, H., & Wang, K. (2021). Postseismic geodetic signature of cold forearc mantle in subduction zones. *Nature Geoscience*, *14*(2), 104–109.

Meade, B. J. (2022). Interseismic masking of fault slip deficit rates by earthquake cycle processes and local block rotations. *Seismological Society of America*, *93*(5), 2770–2775.

Melosh, H., & Raefsky, A. (1981). A simple and efficient method for introducing faults into finite element computations. *Bulletin of the Seismological Society of America*, *71*(5), 1391–1400.

Melosh, H., & Williams Jr, C. (1989). Mechanics of graben formation in crustal rocks: A finite element analysis. *Journal of Geophysical Research: Solid Earth*, *94*(B10), 13961–13973.

Mumme, T., Lamb, S., & Walcott, R. (1989). The raukumara paleomagnetic domain: Constraints on the tectonic rotation of the east coast, north island, new zealand, from paleomagnetic data. *New Zealand journal of geology and geophysics*, *32*(3), 317–326.

Nicol, A., & Beavan, J. (2003). Shortening of an overriding plate and its implications for slip on a subduction thrust, central hikurangi margin, new zealand. *Tectonics*, *22*(6).

Reyners, M. (1998). Plate coupling and the hazard of large subduction thrust earthquakes at the hikurangi subduction zone, new zealand. *New Zealand Journal of Geology and Geophysics*, *41*(4), 343–354.

Reyners, M., Eberhart-Phillips, D., & Bannister, S. (2011). Tracking repeated subduction of the hikurangi plateau beneath new zealand. *Earth and Planetary Science Letters*, *311*(1-2), 165–171.

Ruff, L. J., & Kanamori, H. (1980). Seismicity and the subduction process. *Physics of the Earth and Planetary interiors*, *23*(3), 240–252.

Salmon, M., Kennett, B., Stern, T., & Aitken, A. (2013). The moho in australia and new zealand. *Tectonophysics*, *609*, 288–298.

Schwartz, S. Y., & Rokosky, J. M. (2007). Slow slip events and seismic tremor at circum-pacific subduction zones. *Reviews of Geophysics*, *45*(3).

Stern, T., Stratford, W., & Salmon, M. (2006). Subduction evolution and mantle dynamics at a continental margin: Central north island, new zealand. *Reviews of Geophysics*, *44*(4).

Sutherland, R., Stagpoole, V., Uruski, C., Kennedy, C., Bassett, D., Henrys, S., Scherwath, M., Kopp, H., Field, B., Toulmin, S., et al. (2009). Reactivation of tectonics, crustal underplating, and uplift after 60 myr of passive subsidence, raukumara basin, hikurangi-kermadec fore arc, new zealand: Implications for global growth and recycling of continents. *Tectonics*, *28*(5).

Tesauro, M., Kaban, M. K., & Cloetingh, S. A. (2012). Global strength and elastic thickness of the lithosphere. *Global and Planetary Change*, *90*, 51–57.

Tian, D., Uieda, L., Leong, W. J., Schlitzer, W., Fröhlich, Y., Grund, M., Jones, M., Toney, L., Yao, J., Magen, Y., Tong, J.-H., Materna, K., Belem, A., Newton, T., Anant, A., Ziebarth, M., Quinn, J., & Wessel, P. (2023, September). *PyGMT: A Python interface for the Generic Mapping Tools* (Version 0.10.0). Zenodo. https://doi.org/10.5281/zenodo.8303186

Wallace, L. M. (2020). Slow slip events in new zealand. *Annual Review of Earth and Planetary Sciences*, *48*, 175–203.

Wallace, L. M., Barnes, P., Beavan, J., Van Dissen, R., Litchfield, N., Mountjoy, J., Langridge, R., Lamarche, G., & Pondard, N. (2012). The kinematics of a transition from subduction to strike-slip: An example from the central new zealand plate boundary. *Journal of Geophysical Research: Solid Earth*, *117*(B2).

Wallace, L. M., Beavan, J., McCaffrey, R., & Darby, D. (2004). Subduction zone coupling and tectonic block rotations in the north island, new zealand. *Journal of Geophysical Research: Solid Earth*, *109*(B12).

Wallace, L. M., Cochran, U. A., Power, W. L., & Clark, K. J. (2014). Earthquake and tsunami potential of the hikurangi subduction thrust, new zealand: Insights from paleoseismology, gps, and tsunami modeling. *Oceanography*, *27*(2), 104–117.

Wallace, L. M., Ellis, S., Bannister, S., Henrys, S., Sutherland, R., Bell, R., Townend, J., & Barnes, P. (2010). Subduction systems revealed: Studies of the hikurangi margin. *Eos, Transactions American Geophysical Union*, *91*(45), 417–418.

Wallace, L. M., Hreinsdóttir, S., Ellis, S., Hamling, I., D'Anastasio, E., & Denys, P. (2018). Triggered slow slip and afterslip on the southern hikurangi subduction zone following the kaikōura earthquake. *Geophysical Research Letters*, *45*(10), 4710–4718.

Wallace, L. M., Reyners, M., Cochran, U., Bannister, S., Barnes, P. M., Berryman, K., Downes, G., Eberhart-Phillips, D., Fagereng, A., Ellis, S., et al. (2009). Characterizing the seismogenic zone of a major plate boundary subduction thrust: Hikurangi margin, new zealand. *Geochemistry, Geophysics, Geosystems*, *10*(10).

Webb, T. H., & Anderson, H. (1998). Focal mechanisms of large earthquakes in the north island of new zealand: Slip partitioning at an oblique active margin. *Geophysical journal international*, *134*(1), 40–86.

Williams, C. A., Eberhart-Phillips, D., Bannister, S., Barker, D. H., Henrys, S., Reyners, M., & Sutherland, R. (2013). Revised interface geometry for the hikurangi subduction zone, new zealand. *Seismological Research Letters*, *84*(6), 1066–1073.

Zachariasen, J., Berryman, K., Langridge, R., Prentice, C., Rymer, M., Stirling, M., & Villamor, P. (2006). Timing of late holocene surface rupture of the wairau fault, marlborough, new zealand. *New Zealand Journal of Geology and Geophysics*, *49*(1), 159–174.